AD NUMBER

ADB002276

LIMITATION CHANGES

TO:

Approved for public release; distribution is unlimited.

FROM:

Distribution authorized to U.S. Gov't. agencies only; Test and Evaluation; AUG 1974. Other requests shall be referred to Naval Surface Weapons Center, Dahlgren Laboratory, Code FVR, Dahlgren, VA 22448.

AUTHORITY

usnswc ltr, 26 mar 1984

AD B002276

AUTHORITY: USNSWC
ltr, 26 Mar 84

MDC E1101

INTEGRATED CIRCUIT ELECTROMAGNETIC SUSCEPTIBILITY INVESTIGATION - PHASE II

MOS NAND GATE STUDY

MCDONNELL DOUGLAS ASTRONAUTICS COMPANY - EAST

MCDONNELL DOUGLAS
CORPORATION

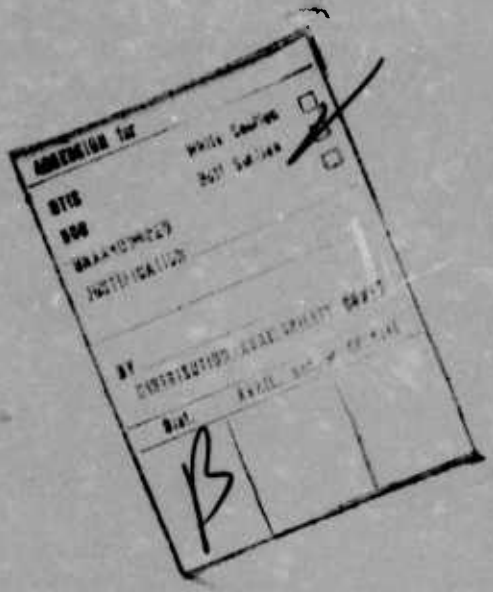
B

COPY NO. 17

INTEGRATED CIRCUIT ELECTROMAGNETIC SUSCEPTIBILITY INVESTIGATION PHASE II.

26 JUL 1974

MDC-E1101

MOS NAND GATE STUDY.

52p.

SUBMITTED TO:
CONTRACTING OFFICER
U.S. NAVAL WEAPONS LABORATORY
DAHLGREN, VA. 22448
CONTRACT NO. N00178-73-C-0362

MCDONNELL DOUGLAS ASTRONAUTICS COMPANY - EAST
Saint Louis, Missouri 63166 (314) 232-0232

MCDONNELL DOUGLAS CORPORATION

403 930

PREFACE

This document is one of eight task-oriented reports prepared under Contract No. N00178-73-C-0362 for the U. S. Naval Weapons Laboratory, Dahlgren, Virginia 22448. The McDonnell Douglas Astronautics Company personnel involved were:

J. M. Roe, Study Manager

J. R. Chott

C. E. Clous

V. R. Ditton

T. A. Niemeier

G. W. Renken

R. D. Von Rohr

J. A. Waite

This report was reviewed by J. R. Cummings.

TABLE OF CONTENTS

List of Pages

Title

i-ii

1 through 53

1. INTRODUCTION AND SUMMARY

The increasing availability of CMOS devices to military system designers presents the possibility of significant differences from bipolar devices vis a vis RF susceptibility. This report documents a preliminary investigation into possible differences between functionally similar devices (the 7400 bipolar NAND gate and the 4011 CMOS NAND gate) at four frequencies: .22, .91, 3.0, and 5.6 GHz. While it is difficult to compare the observed susceptibility modes, it appears that the CMOS 4011 device is slightly less susceptible than the bipolar 7400 device. The underlying susceptibility mechanism can be explained by rectification of the RF signal in parasitic and protective pn junctions as in the bipolar devices [1], but the circuit reaction to these rectified currents and voltages is different.

2. MOS SUSCEPTIBILITY MEASUREMENTS

In as much as MOS technology represents a growing segment of the integrated circuit world (one recent estimate forecasts CMOS will outstrip TTL in usage by 1976), it has been planned from the inception of the IC program to study RF susceptibility of MOS devices. As the measurement techniques and results from the bipolar studies [1, 2, 3, 4] matured, it became highly desirable to determine whether a system designer could gain a significant improvement in overall system RF hardness by using MOS technology in lieu of bipolar technology. This part of the program was designed to probe that possibility by measuring a CMOS NAND gate which is functionally identical to the previously-studied 7400 bipolar NAND gate.

2.1 Experimental Plan - Devices manufactured by the MOS technology employ significantly different fabrication techniques than those used in bipolar devices. MOS technology can be roughly divided into three main subdivisions: p-channel, n-channel and complementary. In addition there are many subtechnologies: silicon gate, metal gate, dielectric isolated, etc. The complementary MOS devices (CMOS) include both n-channel and p-channel devices on the same chip making them particularly attractive for study. Most digital CMOS devices have been of the enhancement mode type. The CMOS technology can also be used to manufacture both digital and linear devices on the same chip. For these reasons a CMOS NAND gate (4011) was chosen for study.

2.1.1 CMOS NAND Gate - The 4011 is a quad 2-input NAND gate having the same schematic representation as the bipolar 7400 NAND gate, although they are not pin-for-pin interchangeable. The circuit diagram for this NAND gate is shown in figure 1. Also depicted in figure 1 are the current and voltage conventions used for this device throughout this report. A photomicrograph of one of the four NAND gates on the 4011 chip is shown in figure 2. CMOS devices have very high DC input impedance ($10^{12}\Omega$ and 5 pf), very low quiescent power drain (5nW), high noise

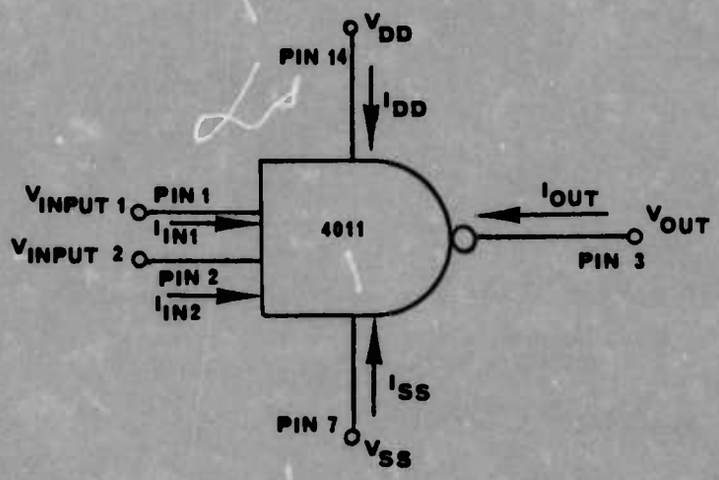

4011 SCHEMATIC DIAGRAM

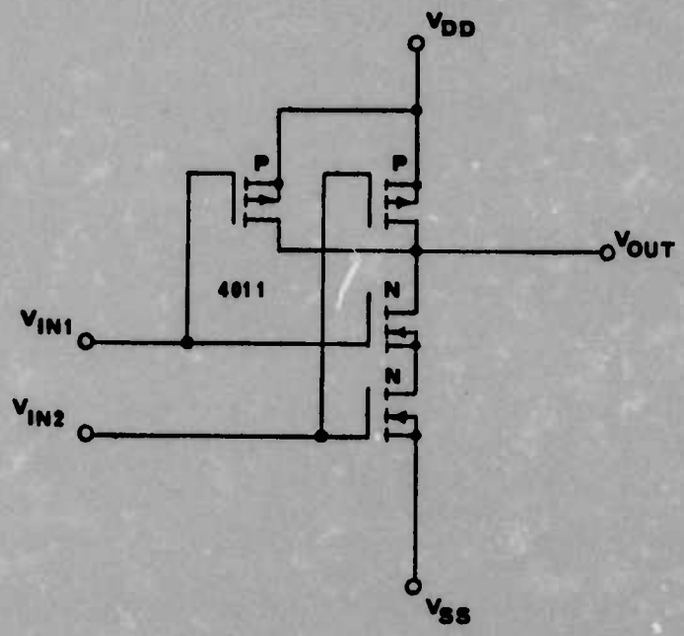

4011 CIRCUIT DIAGRAM

Figure 1 4011 SCHEMATIC AND CIRCUIT DIAGRAM

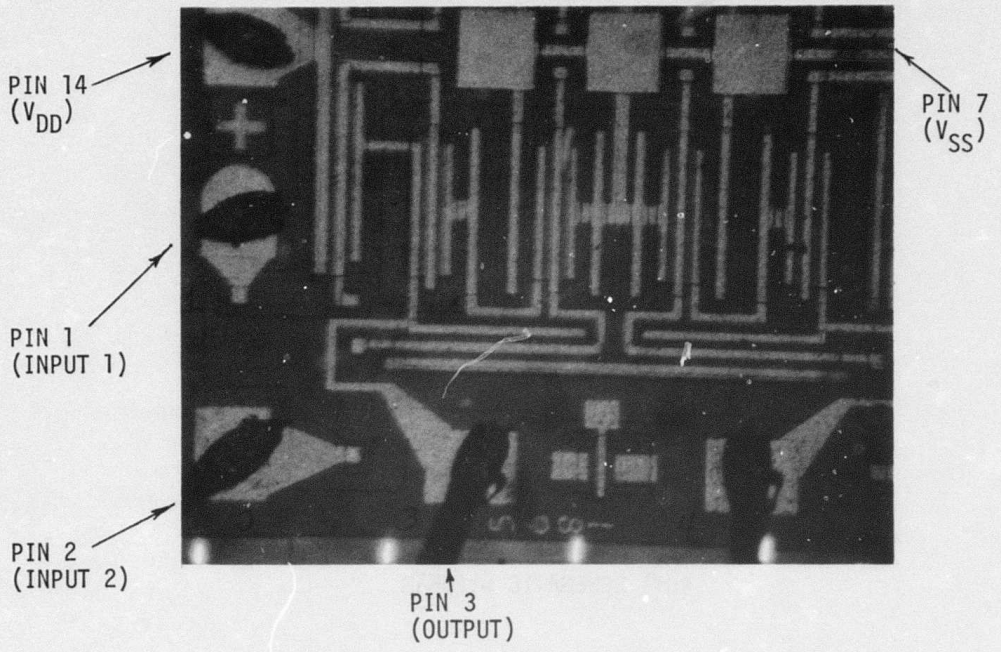

Figure 2 PHOTOMICROGRAPH OF CMOS 4011 NAND GATE

immunity (30% of V_{DD}) and the capability of operating from power supplies over the range of 3 → 15 volts. Most CMOS devices are now fabricated with protective circuits on all gate inputs and some outputs to integrate and clamp the device voltage to a safe level. The breakdown voltage of the gate oxide is generally in the order of 70 to 100 volts and because of the high resistance of this oxide, even a very low energy source (static charge) is capable of damaging a device without protection. Because of the low RF time constants of these protective circuits, they have no noticeable effect on circuit speed and do not interfere with normal circuit operation.

2.1.2 4011 Test Circuit - Only one of the four NAND gates on the 4011 chip was investigated for RF susceptibility. A power supply voltage of 5 volts was chosen for 4011 testing for ease of comparison with the 7400 data. Voltage and current were measured for each of the five DC ports of the NAND gate. The bias circuitry for the 4011 for all input/output conditions is shown in figure 3. The input loading was chosen to simulate the nominal resistance of another CMOS device. The output loading for each logic state was determined for the maximum source and sink current specified. The automated measurement system used for 4011 interference testing is shown in figure 4. This measurement system facilitates the collection of the large amounts of data required for accurate RF susceptibility characterization of ICs. The measurement system is discussed in the IC Susceptibility Test and Measurement Systems Report [5]. The schematic diagram for the 4011 interference measurement system is shown in figure 5.

There are five possible RF entry ports into the 4011 device: two identical inputs, an output, the power supply (V_{DD}) and ground (V_{SS}). Since the inputs are identical, the duplicate input port was not used for RF injection. All RF measurements were performed with the 4011 DC biased in either the output high or the output low case. No dynamic switching conditions were considered. Figure 6 shows the flow diagram for the 4011 RF interference testing.

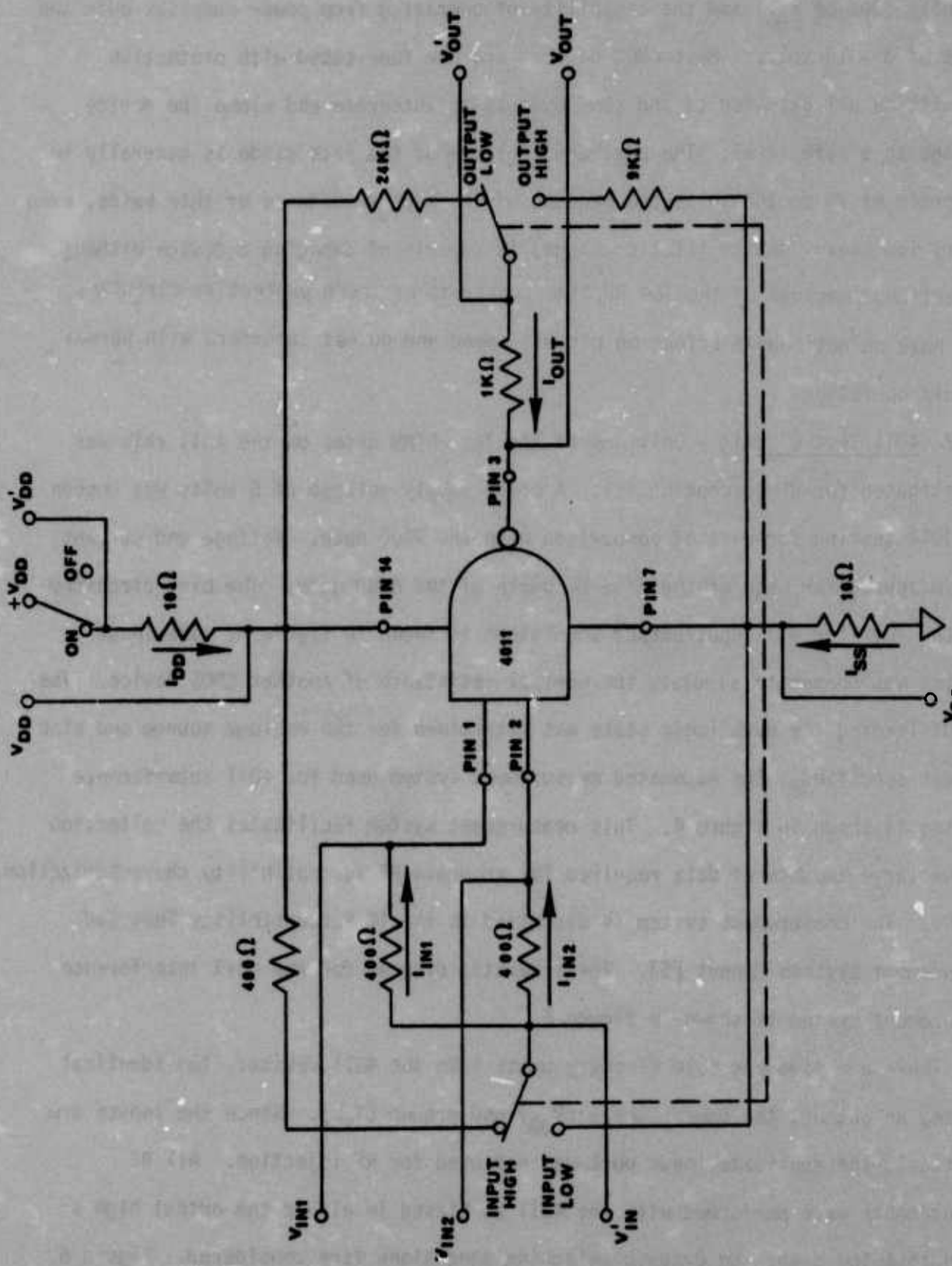

Figure 3 4011 BIAS CIRCUITRY

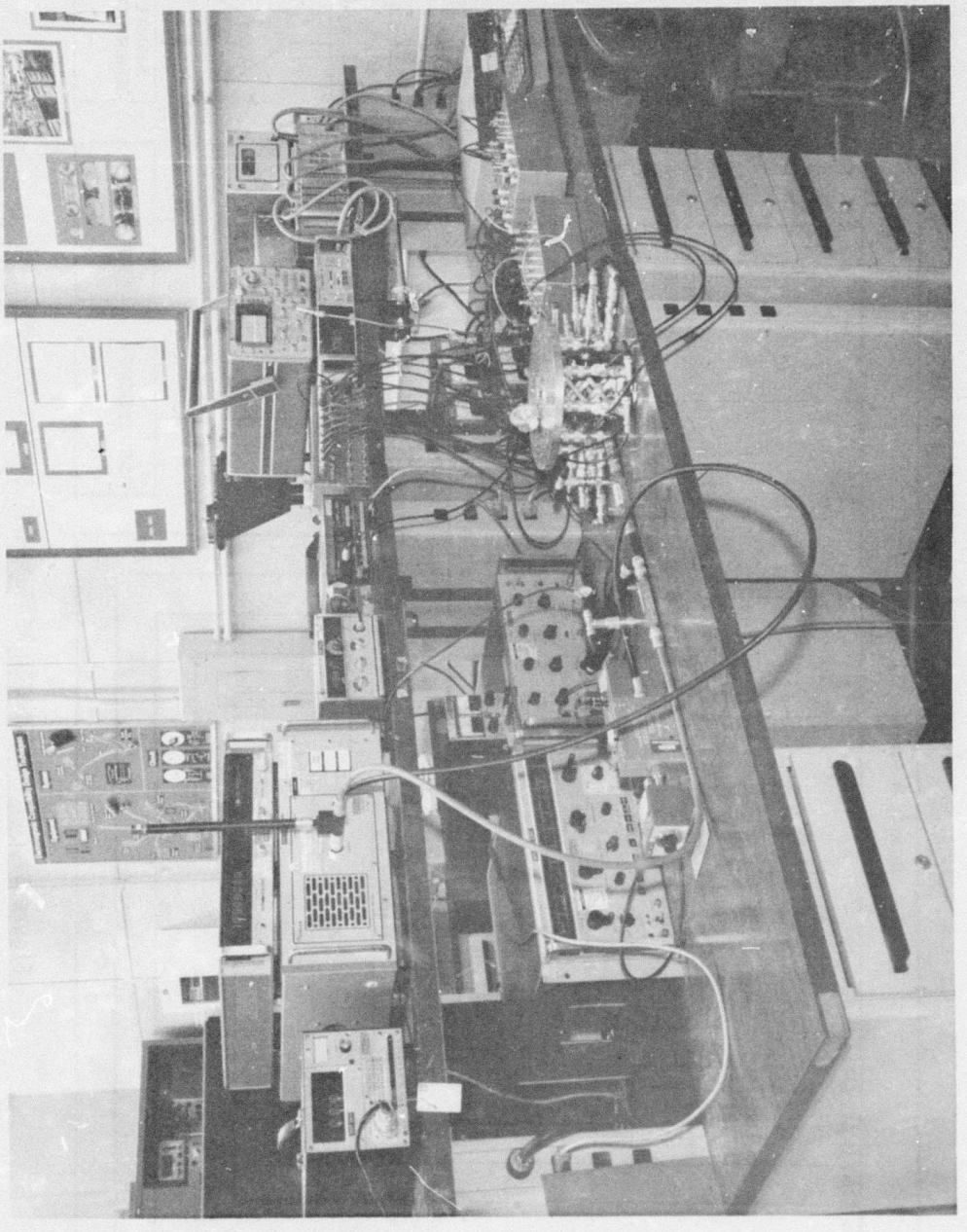

Figure 4 4011 AUTOMATED MEASUREMENT TEST SETUP

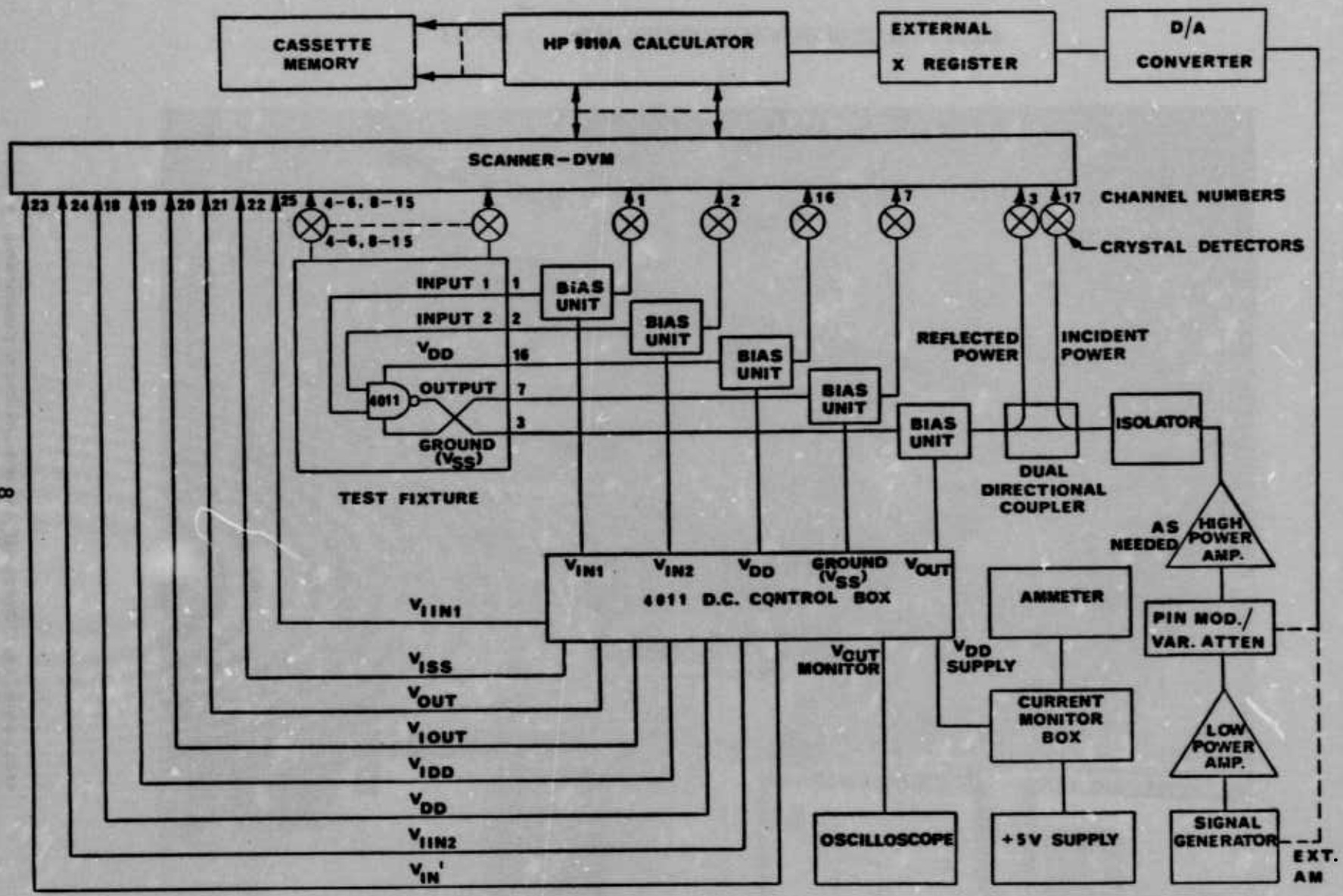

Figure 5 4011 AUTOMATED MEASUREMENT SYSTEM SCHEMATIC

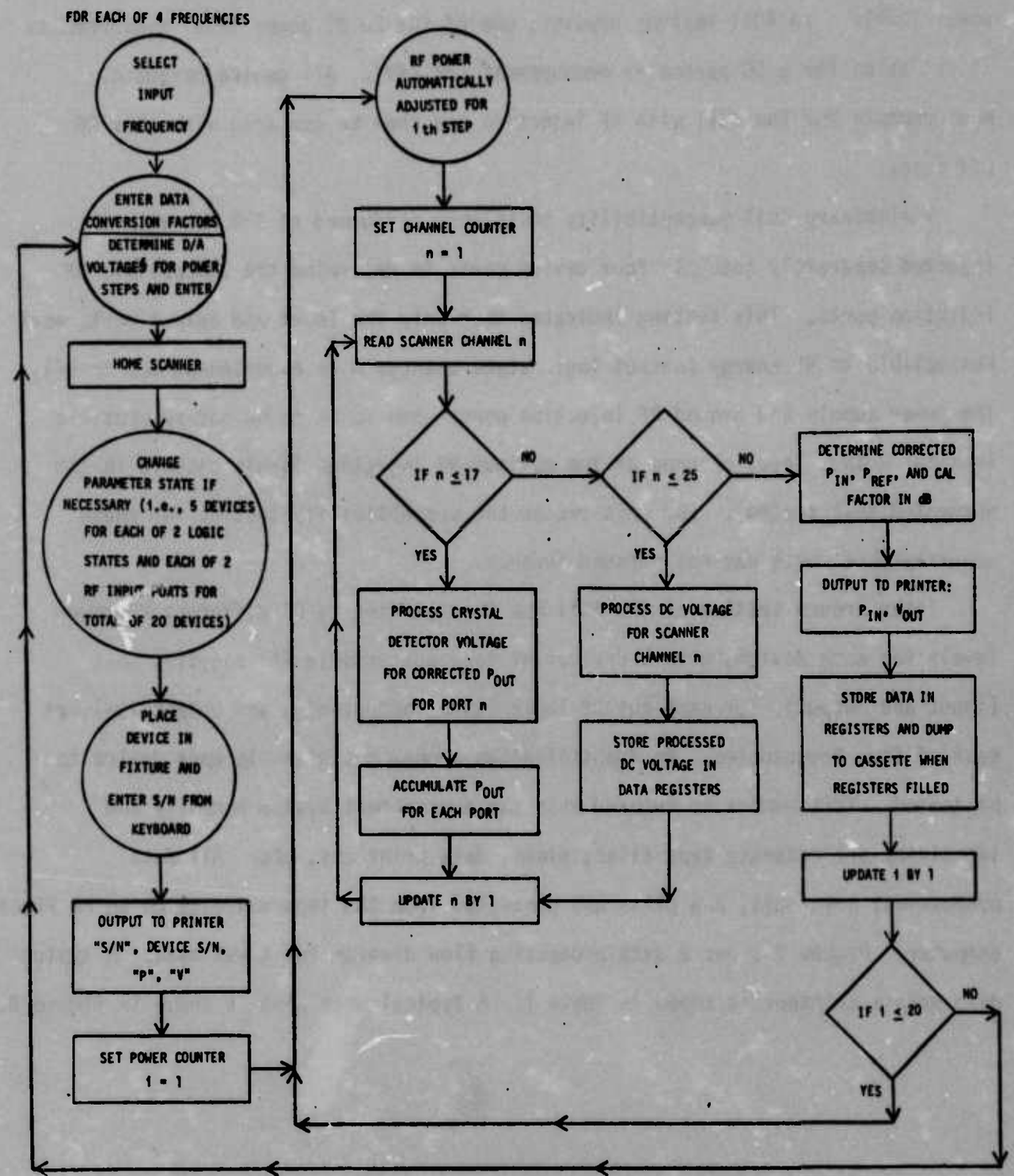

Figure 6 4011 INTERFERENCE TEST FLOW DIAGRAM

As in 7400 interference testing, device parameters were measured for 20 RF power levels. In 4011 testing however, one of the 20 RF power level measurements is set aside for a DC parameter measurement (RF off). All device parameter measurements for the 4011 with RF injection can then be compared with this RF off case.

Preliminary 4011 susceptibility tests were performed at 910 MHz with RF injected separately into all four device ports to determine the susceptible RF injection ports. This testing indicated that only the input and output ports were susceptible to RF energy (output logic state changes were experienced due to RF). The power supply and ground RF injection ports were found to be not susceptible (minimal output level changes at the maximum RF injection levels capable in the automated test system). For this reason the susceptibility testing for these unsusceptible ports was not pursued further.

Interference testing of the 4011 was then limited to 20 different RF power levels for each device, with 5 devices at each susceptible RF injection port (input and output), for each output logic state (output high and output low), at each of four frequencies. An identification number was given to each device to be tested. This number is entered into the measurement system manually and identifies all cassette tape files, plots, data printouts, etc. All data processing, printouts, and plots are generated from the tape cassette on an HP 9830A computer. Figure 7 shows a data processing flow diagram for these data. A typical data matrix printout is shown in Table 1. A typical data plot is shown in figure 8.

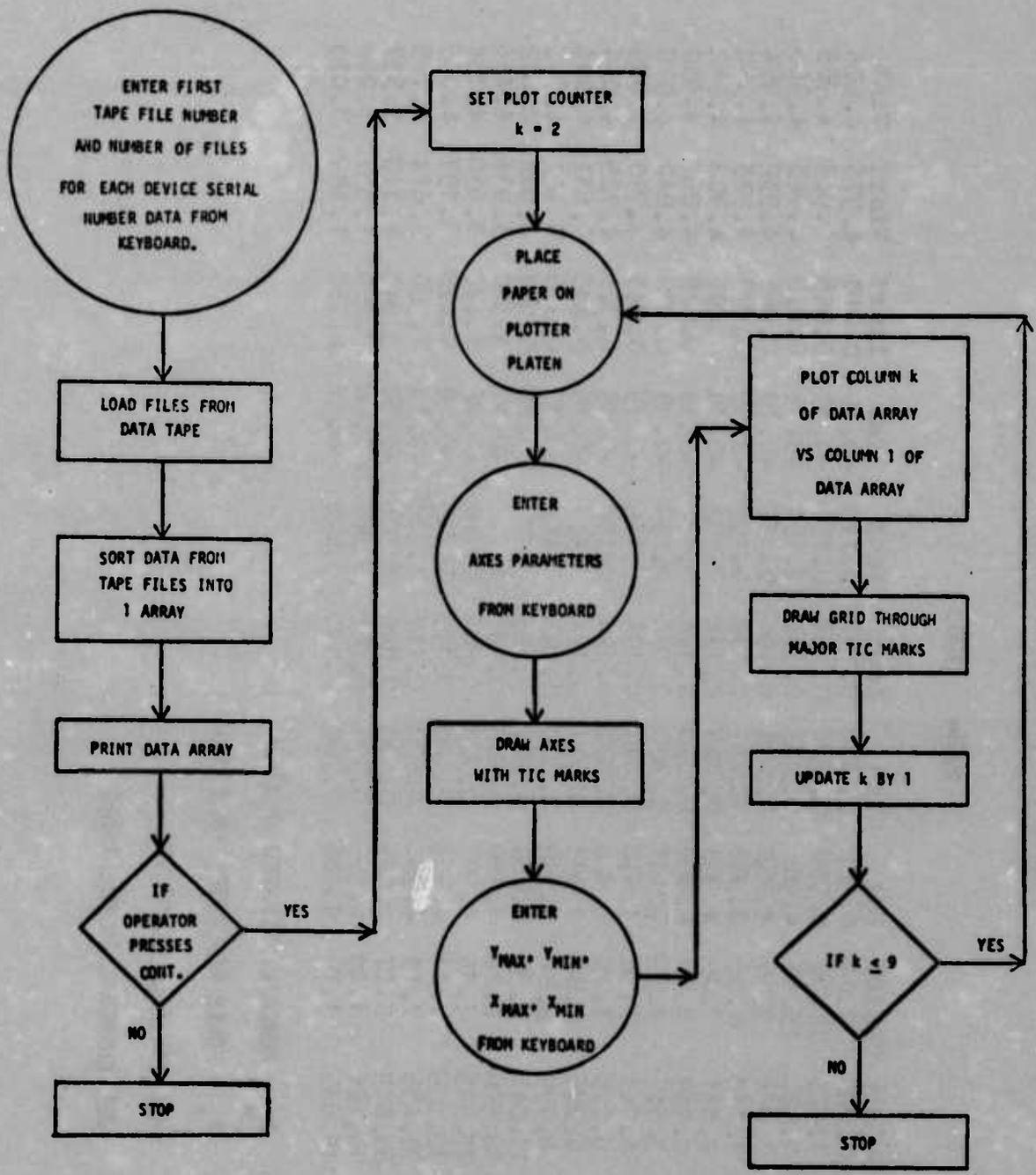

Figure 7 4011 INTERFERENCE TEST DATA REDUCTION FLOW DIAGRAM

Table 1 TYPICAL 4011 DATA PRINTOUT

S/N= 1203

Pd(mW)	Pr(mW)	CF(dB)	Vdd	Idd	Iout	Vout	Iss	Iinrf	Vinrf	Vin1
-0.000	0.000	0.00	4.988	0.300	0.194	0.150	-0.19	0.010	4.976	4.976
0.007	1.673	24.06	4.988	0.300	0.194	0.151	-0.19	0.045	4.949	4.963
0.091	1.828	13.68	4.988	0.300	0.194	0.151	-0.19	0.050	4.943	4.960
0.268	2.074	9.86	4.988	0.300	0.194	0.152	-0.19	0.065	4.932	4.954
0.413	2.244	8.55	4.988	0.300	0.194	0.152	-0.19	0.078	4.923	4.950
0.719	2.531	7.05	4.988	0.300	0.194	0.152	-0.19	0.095	4.908	4.942
1.291	2.949	5.70	4.988	0.300	0.194	0.153	-0.19	0.125	4.883	4.930
2.371	3.547	4.55	4.988	0.300	0.194	0.154	-0.19	0.178	4.842	4.910
3.988	4.247	3.78	4.988	0.200	0.194	0.156	-0.19	0.243	4.790	4.883
6.260	5.079	3.25	4.988	0.300	0.194	0.158	-0.19	0.325	4.725	4.851
10.010	6.276	2.84	4.988	0.200	0.194	0.161	-0.19	0.443	4.631	4.804
17.000	8.739	2.64	4.988	0.300	0.193	0.168	-0.19	0.665	4.451	4.713
26.759	11.047	2.35	4.988	0.200	0.193	0.177	-0.20	0.868	4.288	4.632
47.871	16.930	2.22	4.988	0.200	0.191	0.223	-0.22	1.310	3.936	4.456
72.187	23.325	2.16	4.987	0.300	0.189	0.308	-0.28	1.693	3.630	4.304
114.368	33.559	2.11	4.986	0.400	0.179	0.549	-0.39	2.228	3.197	4.089
180.791	50.455	2.11	4.984	0.600	0.141	1.333	-0.59	2.960	2.614	3.795
266.745	68.819	2.07	4.984	0.600	0.105	2.505	-0.60	3.543	2.140	3.557
419.195	96.626	1.99	4.985	0.500	0.072	3.068	-0.50	4.280	1.557	3.266
655.173	116.647	1.79	4.985	0.500	0.110	3.006	-0.46	4.750	1.189	3.075

P_d = POWER DISSIPATED IN CHIP

P_r = POWER REFLECTED FROM CHIP

ALL VOLTAGES IN VOLTS

ALL CURRENTS IN MILLIAMPS

INTEGRATED CIRCUIT SUSCEPTIBILITY

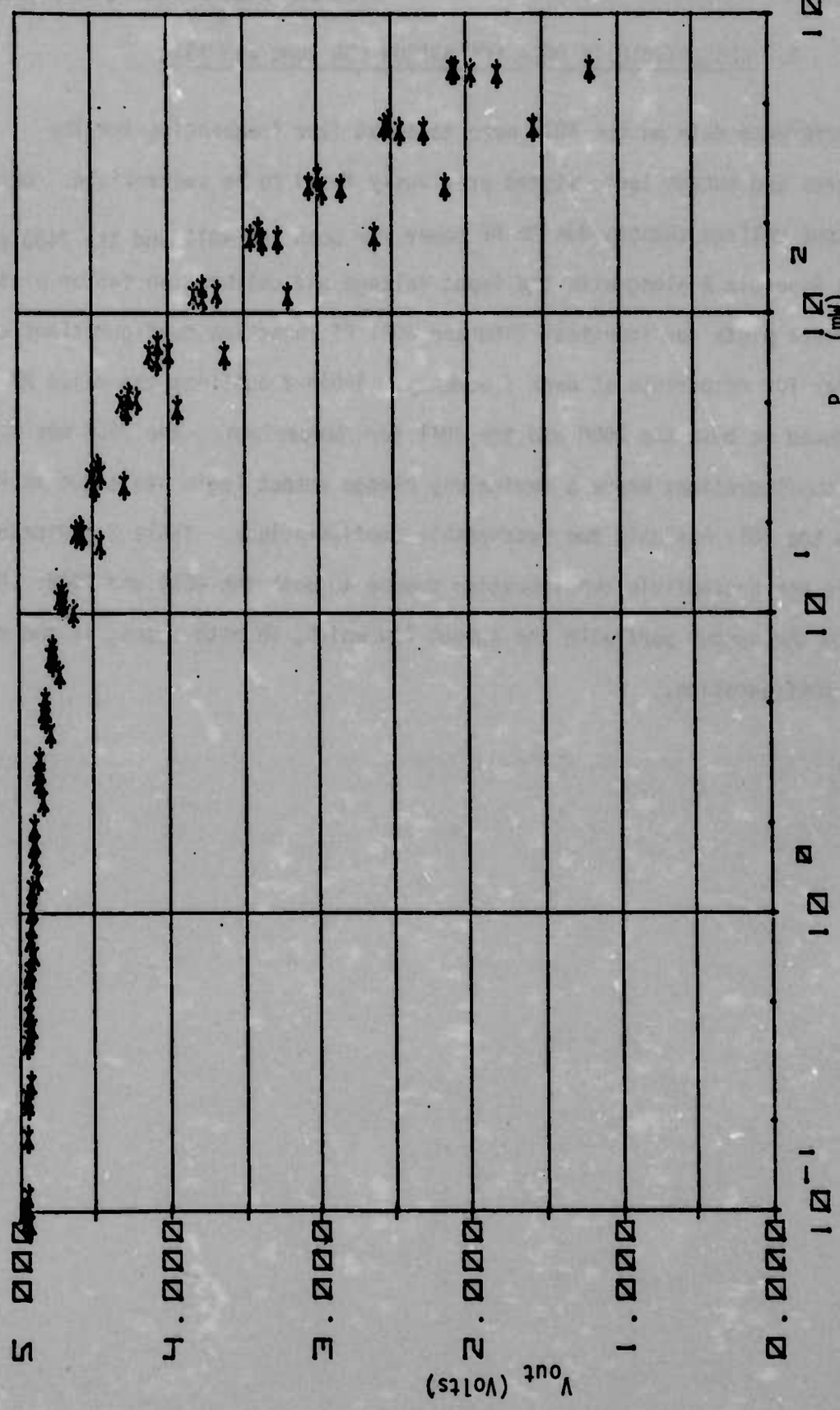

Figure 8 TYPICAL 4011 DATA PLOT

3. SUSCEPTIBILITY DATA COMPARISON FOR 7400 and 4011

RF interference data on the 4011 were taken at four frequencies for the injection ports and output logic states previously found to be susceptible. Data plots of output voltage changes due to RF power for both the 4011 and the 7400 are tabulated in Appendix A along with the input voltage and calibration factor plots. The interference plots for identical 7400 and 4011 RF injection configurations are shown together for comparison at each frequency. Table 2 outlines the major RF effects produced on both the 7400 and the 4011 for comparison. The 7400 has four susceptible configurations where a device may change output logic state due to RF energy while the 4011 has only two susceptible configurations. Table 2 indicates that there is one susceptible configuration common to both the 4011 and 7400: RF injected into the output port with the output low which, in both cases, is the most susceptible configuration.

TABLE 2

7400/4011 RF SUSCEPTIBILITY COMPARISON

RF INJECTION CONDITIONS	7400 RESPONSE	4011 RESPONSE
RF INTO INPUT - OUTPUT HIGH	OUTPUT GOES LOW	OUTPUT DECREASES ≈ .5V
RF INTO INPUT - OUTPUT LOW	NO EFFECT	OUTPUT GOES HIGH
RF INTO OUTPUT - OUTPUT HIGH	SOME OUTPUTS GO LOW	OUTPUT DECREASES ≈ .4V
RF INTO OUTPUT - OUTPUT LOW	SOME OUTPUTS GO HIGH	OUTPUT GOES HIGH
RF INTO POWER SUPPLY OUTPUT HIGH	OUTPUT GOES HIGHER	NOT SUSCEPTIBLE
RF INTO POWER SUPPLY OUTPUT LOW	OUTPUT INCREASES ≈ .5V	NOT SUSCEPTIBLE
RF INTO GROUND - OUTPUT HIGH	SOME OUTPUTS GO LOW	NOT SUSCEPTIBLE
RF INTO GROUND - OUTPUT LOW	SOME OUTPUTS INCREASE ≈1V	NOT SUSCEPTIBLE

4. SUSCEPTIBILITY DATA ANALYSIS

The bipolar rectification model for RF effects, is based on RF signals being rectified at various device pn junctions. The bipolar RF effects model is a representation of an RF generated current source which can be characterized as shown in figure 9. In the case of the 7400, there are many pn junctions on the 7400 chip, as well as many parasitics, as shown in figure 10. Each pn junction on the chip can be replaced with the equivalent circuit of the model.

Numerous parasitic and protective diodes are present on the 4011 chip as shown in figure 11. The parasitic junctions are inherent junctions formed in the actual device fabrication due to isolation techniques. The manner in which parasitic junctions are formed in a representative CMOS device is shown in figure 12. Protective diodes in the case of CMOS devices are intentionally diffused junctions into the over all device structure forming an input limiter circuit that provides protection against static voltages. These diodes suggest a CMOS rectification theory for RF effects similar to the 7400 RF effects rectification theory [1]. Both the input and output circuitry of the 4011 are analyzed for their most susceptible configurations using the concepts of the bipolar rectification model.

4.1 4011 Input Circuit Analysis - The DC bias circuitry for the 4011 NAND gate with the output low is shown in figure 13 for RF injected into the input port. With high levels of RF injected into the input port, the input voltage decreases to a low input state level (See Appendix A). The output voltage follows the input voltage changes and increases with increasing incident RF power to a specified high output state. The input current also rises due to the incident RF energy (from below our measurement system capability to milliamps in some cases). This current is directly attributable to the injected RF because the normal DC current into the gate with no RF is approximately 10 pA. Using the concepts of the bipolar rectification theory, pertinent pn junctions in the 4011 input circuit are replaced with RF effects models

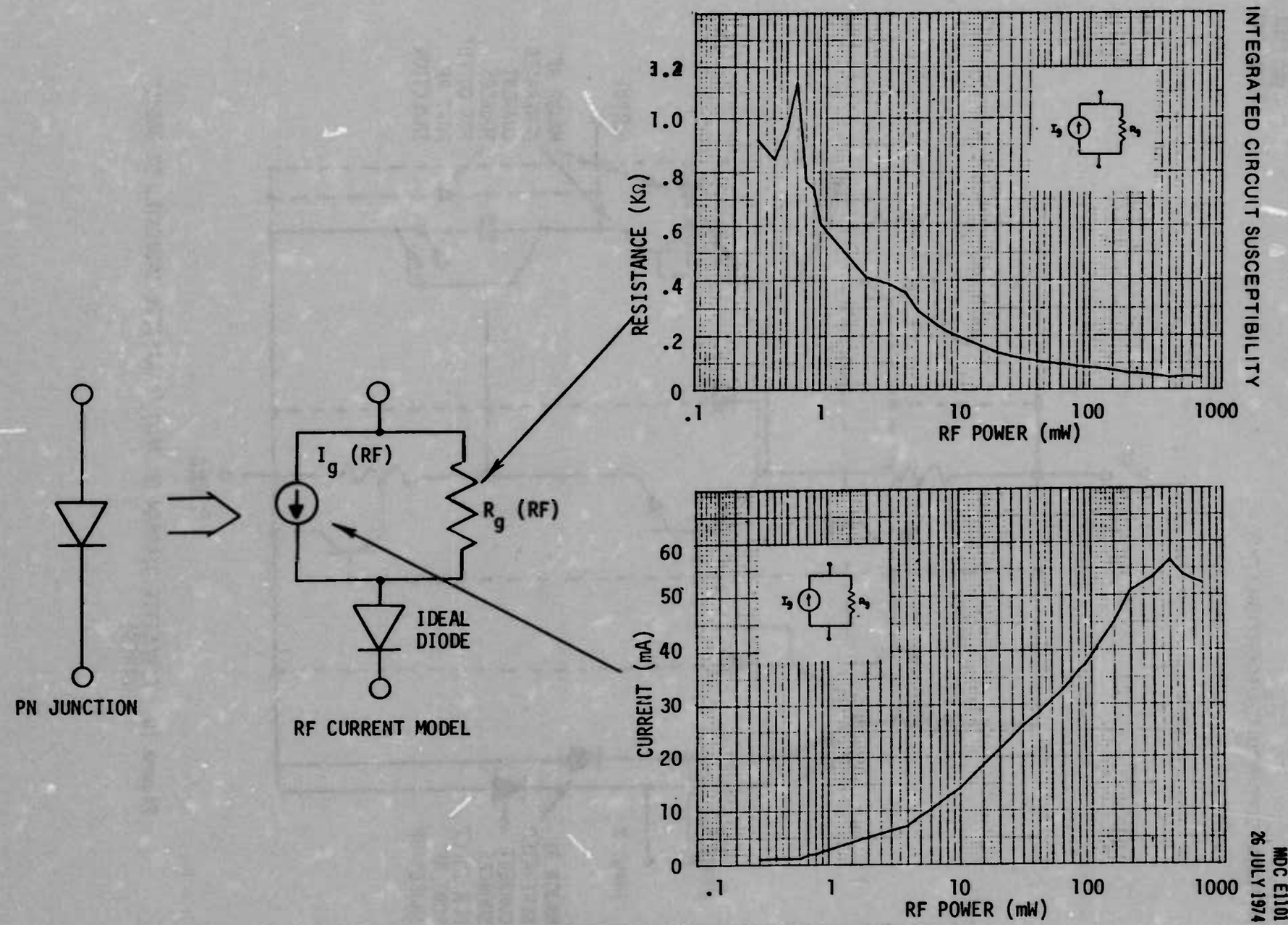

Figure 9 RF MODEL OF DIODE WITH COMPONENT CHARACTERIZATION CURVES AS A FUNCTION OF RF POWER

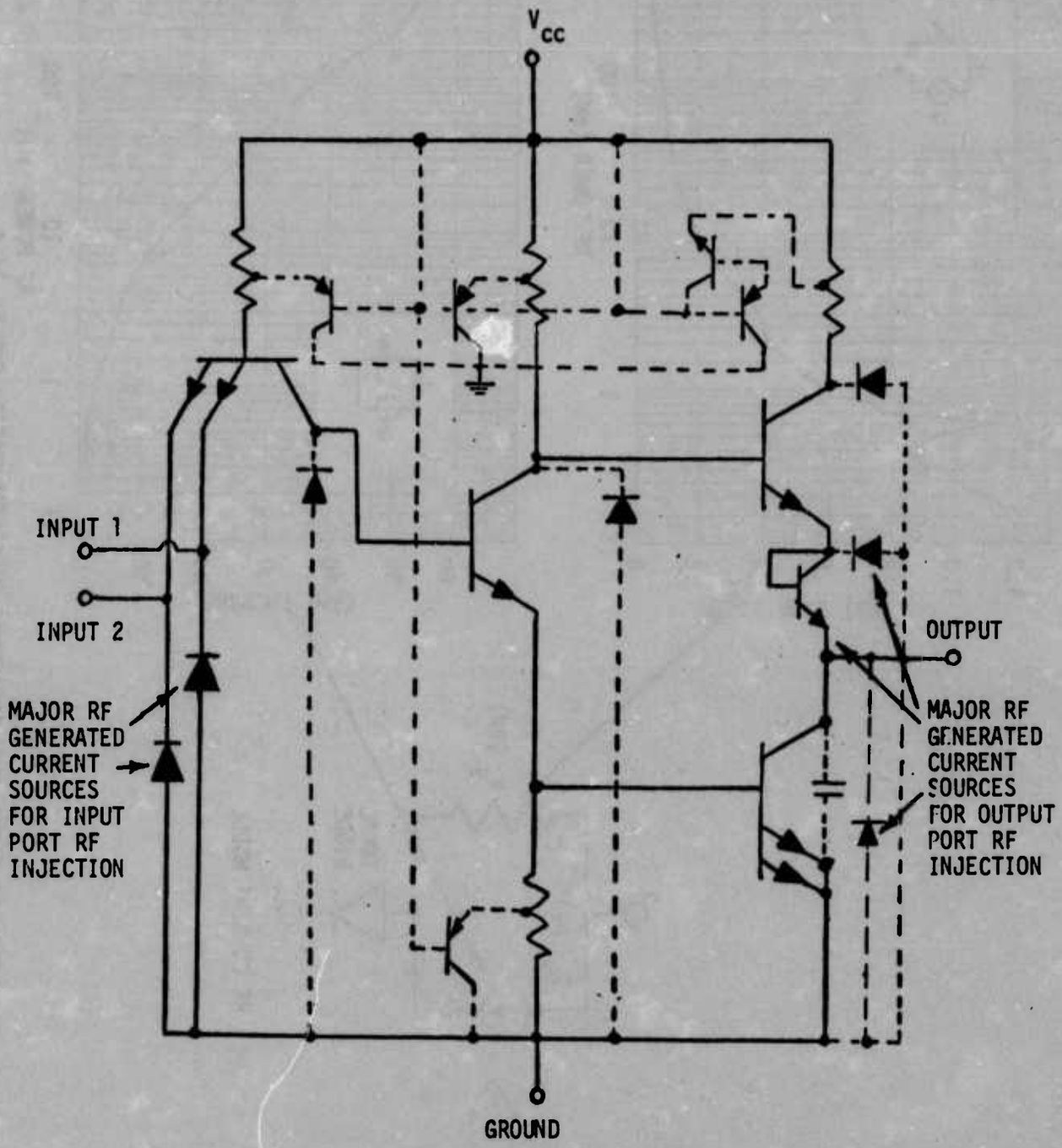

Figure 10 PARASITIC DIAGRAM OF 7400 (PARASITIC INDICATED BY DASHED LINES)

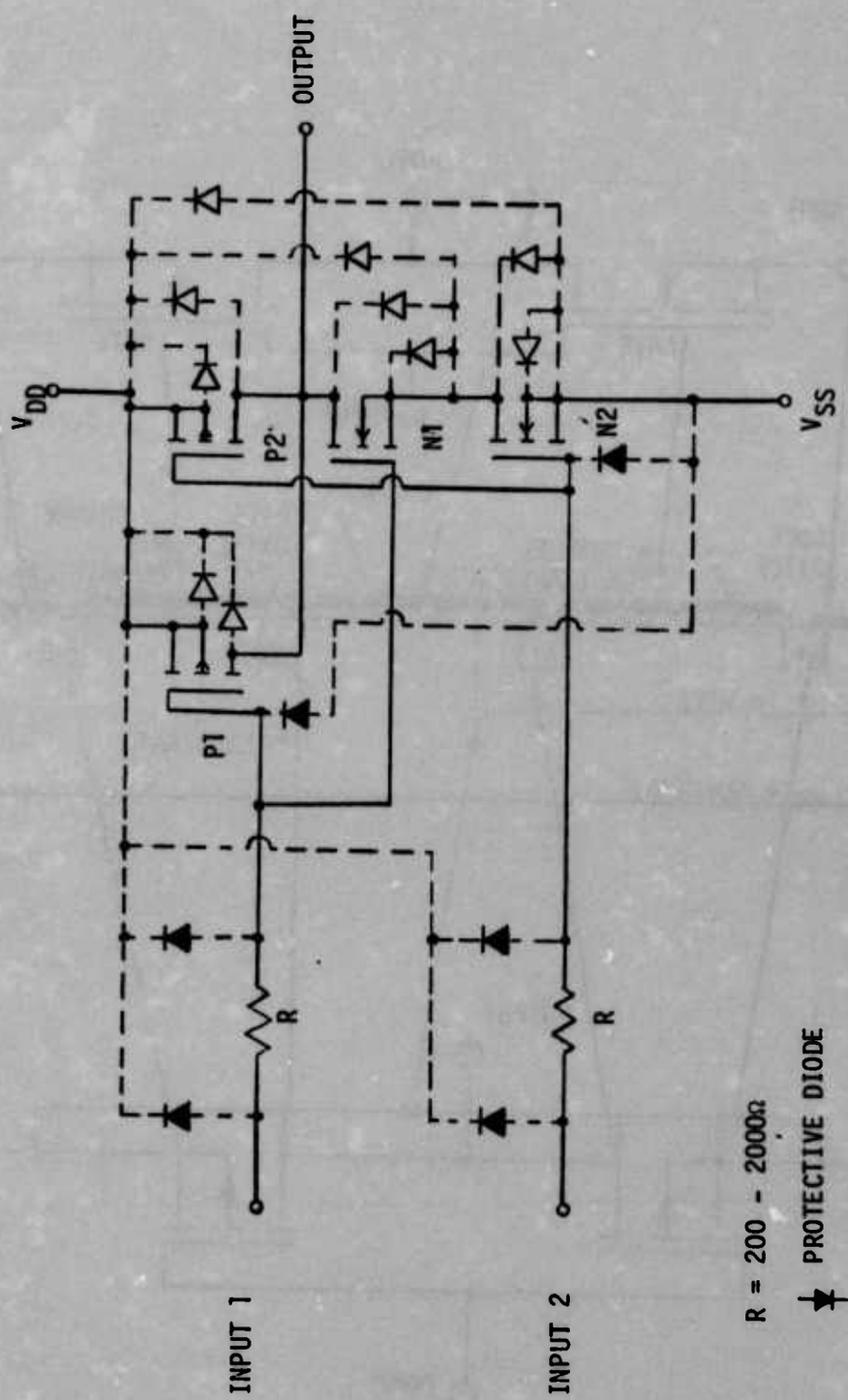

Figure 11 4011 CIRCUIT DIAGRAM SHOWING ALL PN JUNCTIONS (PARASITIC AND PROTECTIVE JUNCTIONS INDICATED BY DASHED LINES)

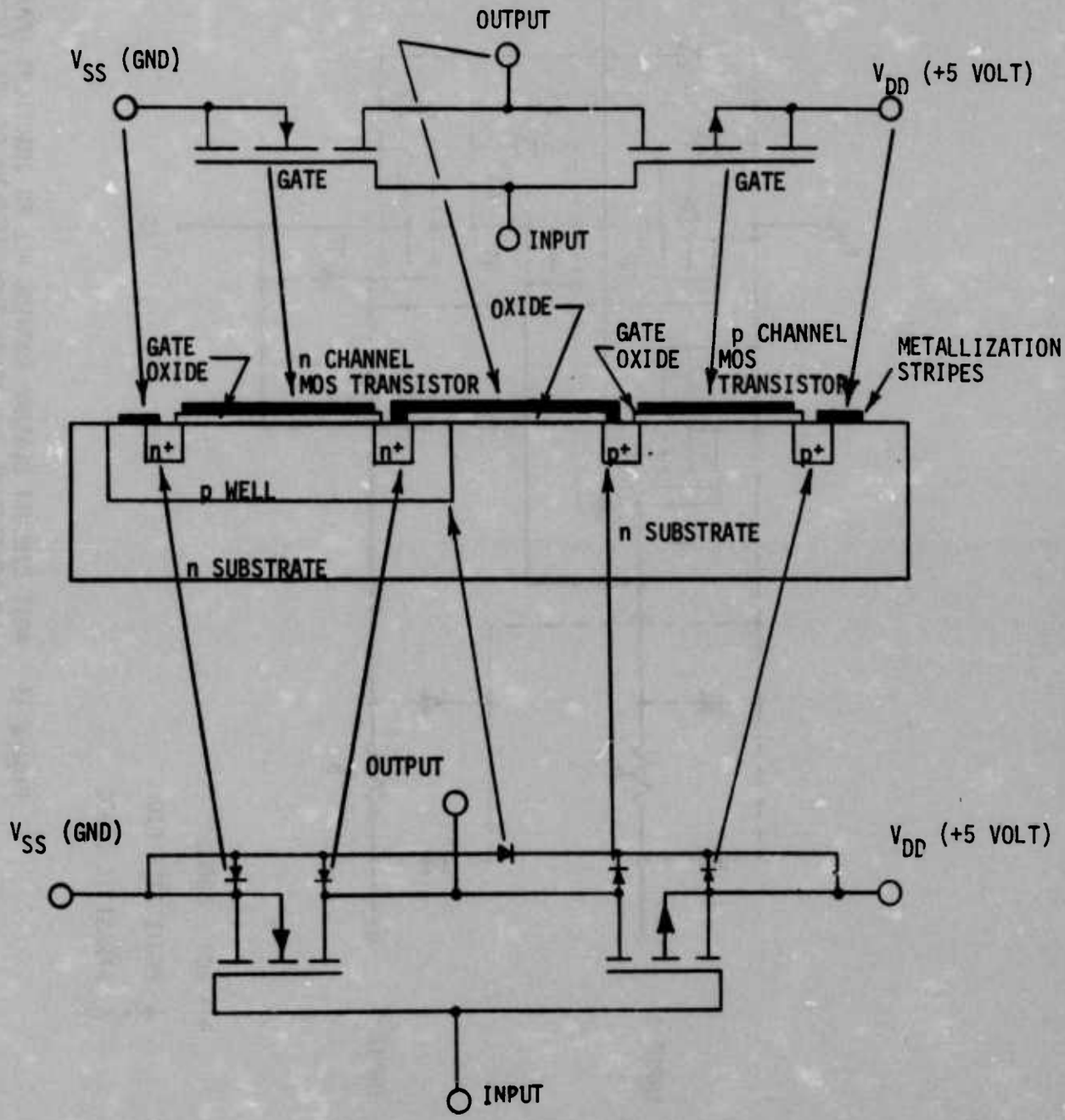

Figure 12 CROSS-SECTION OF TYPICAL CMOS DEVICE SHOWING THE PARASITIC JUNCTIONS AND THEIR SCHEMATIC REPRESENTATION

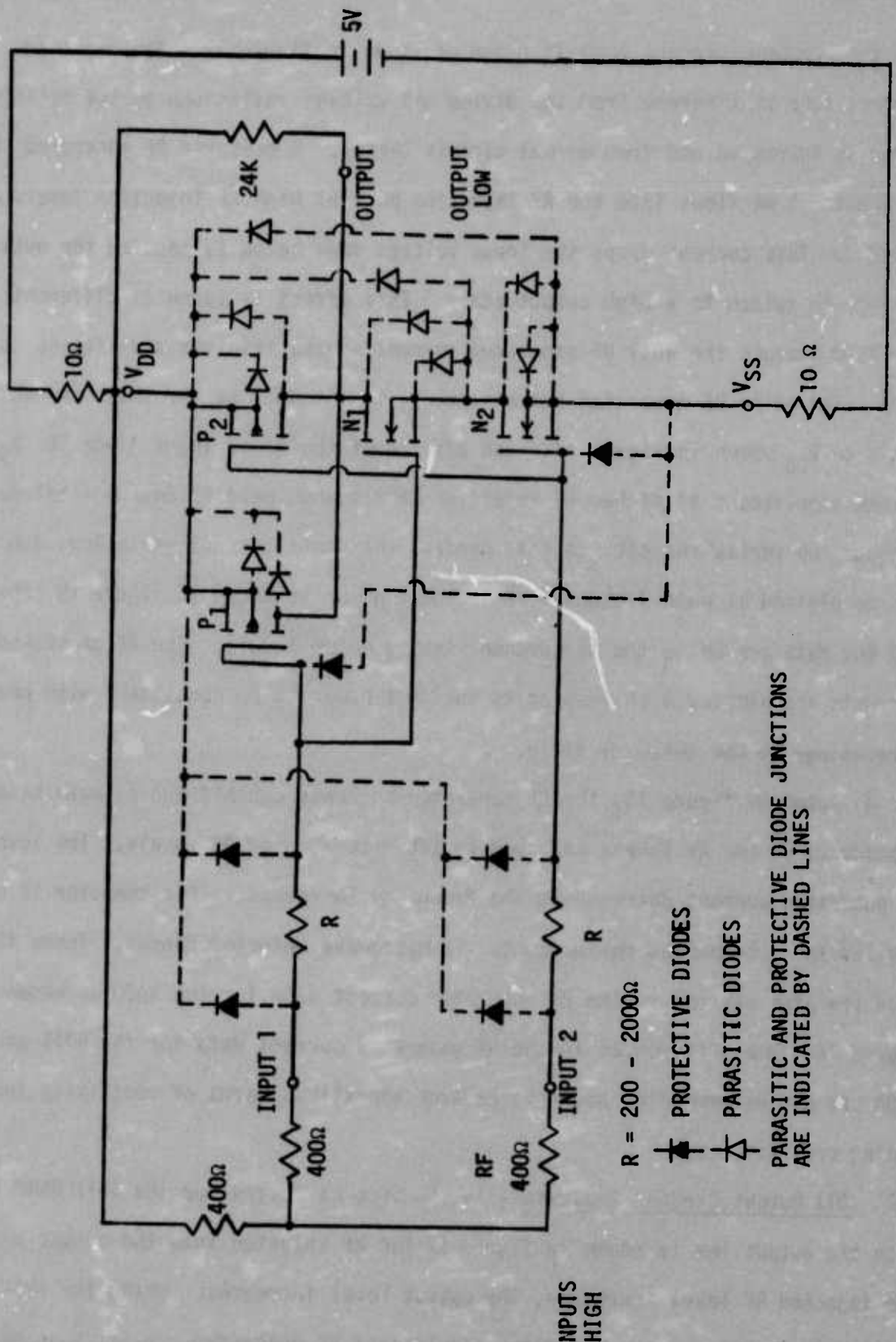

Figure 13 SCHEMATIC DIAGRAM OF 4011 TEST SETUP FOR RF INJECTED INTO THE INPUT PORT WITH THE OUTPUT LOW

and the proposed current loop is drawn as shown in figure 14. The proposed current loop is inferred from the device and voltage variations as the incident RF power is increased and from normal circuit theory. A measured RF generated current of about 3.5 mA flows into the RF injection port at high RF injection levels at 220 MHz. This current drops the input voltage down below 2V causing the output voltage to switch to a high output state. This effect is somewhat different from the 7400 because the 4011 RF generated current source involves a different current loop. The major RF generated current source in the 4011 is the input protective diode to V_{DD} shown in figure 14. The effects of the lower input diode (to V_{SS}) may become significant at higher RF injection levels when more RF energy is allowed through the series resistor to this diode. The input current variations due to RF can be plotted at each frequency vs incident power as shown in figure 15 (the 5.6 GHz data are below the measurement system noise level). The RF generated currents are plotted with respect to incident power to be consistent with present terminology in the detector field.

As shown in figure 15, the RF generated currents exhibit approximate square law dependence at low RF levels and tend to saturate at high RF levels. The levels of RF generated current decrease as the frequency increases. This behavior is quite similar to well-founded measurements for microwave detector diodes. These 4011 data are also similar to the RF generated current data for the 7400 as shown in figure 16. The differences in the RF generated current data for the 4011 and the 7400 are due to generator source impedance variations, area of rectifying junctions, doping profiles, etc.

4.2 4011 Output Circuit Analysis - The DC bias circuitry for the 4011 NAND gate with the output low is shown in figure 17 for RF injected into the output port. As the injected RF level increases, the output level increases. Using the rectification model and the voltage-current data, significant RF generated current sources are

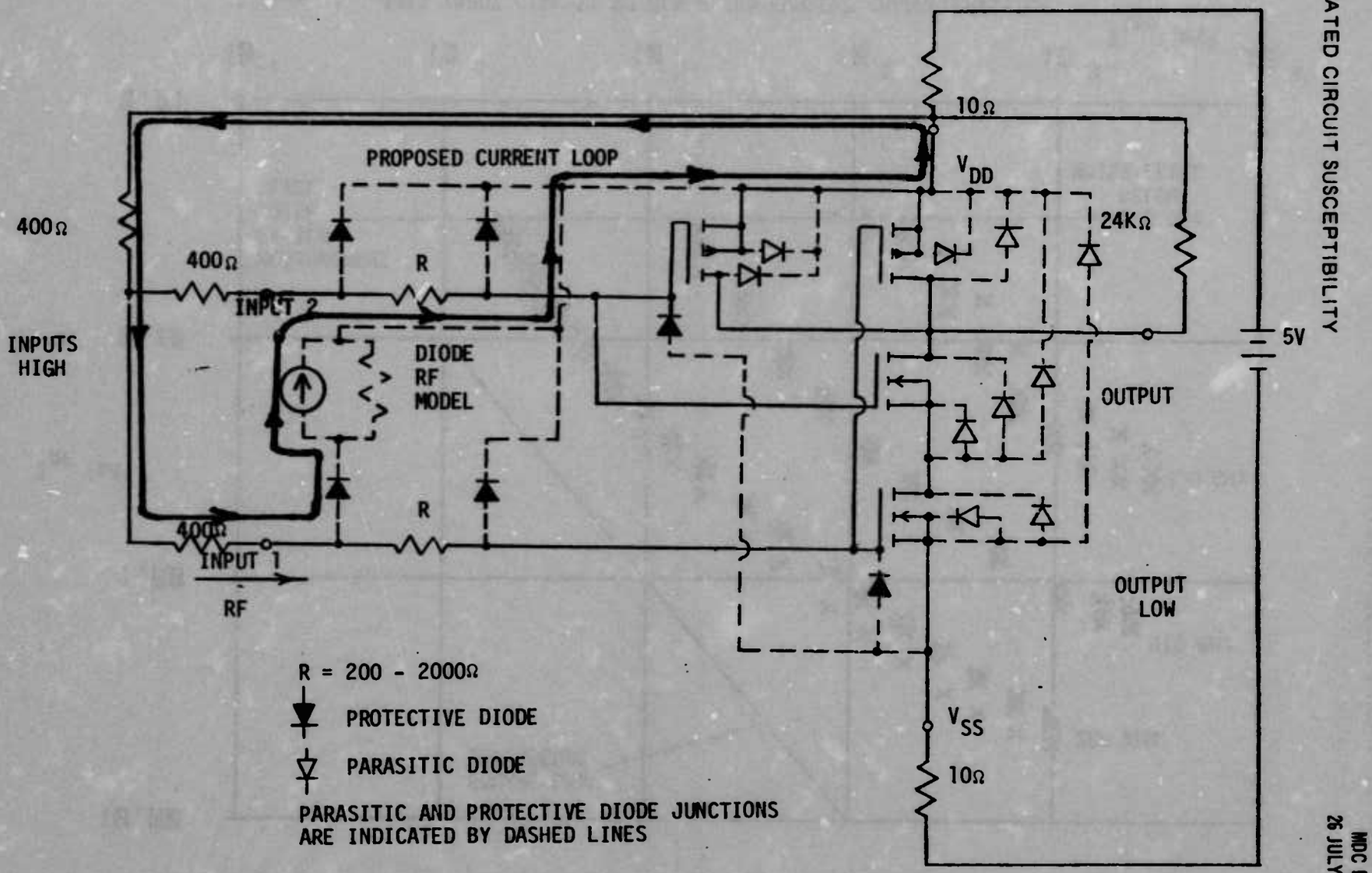

Figure 14 4011 TEST CIRCUIT FOR INPUT RF INJECTION SHOWING RF GENERATED CURRENT SOURCES

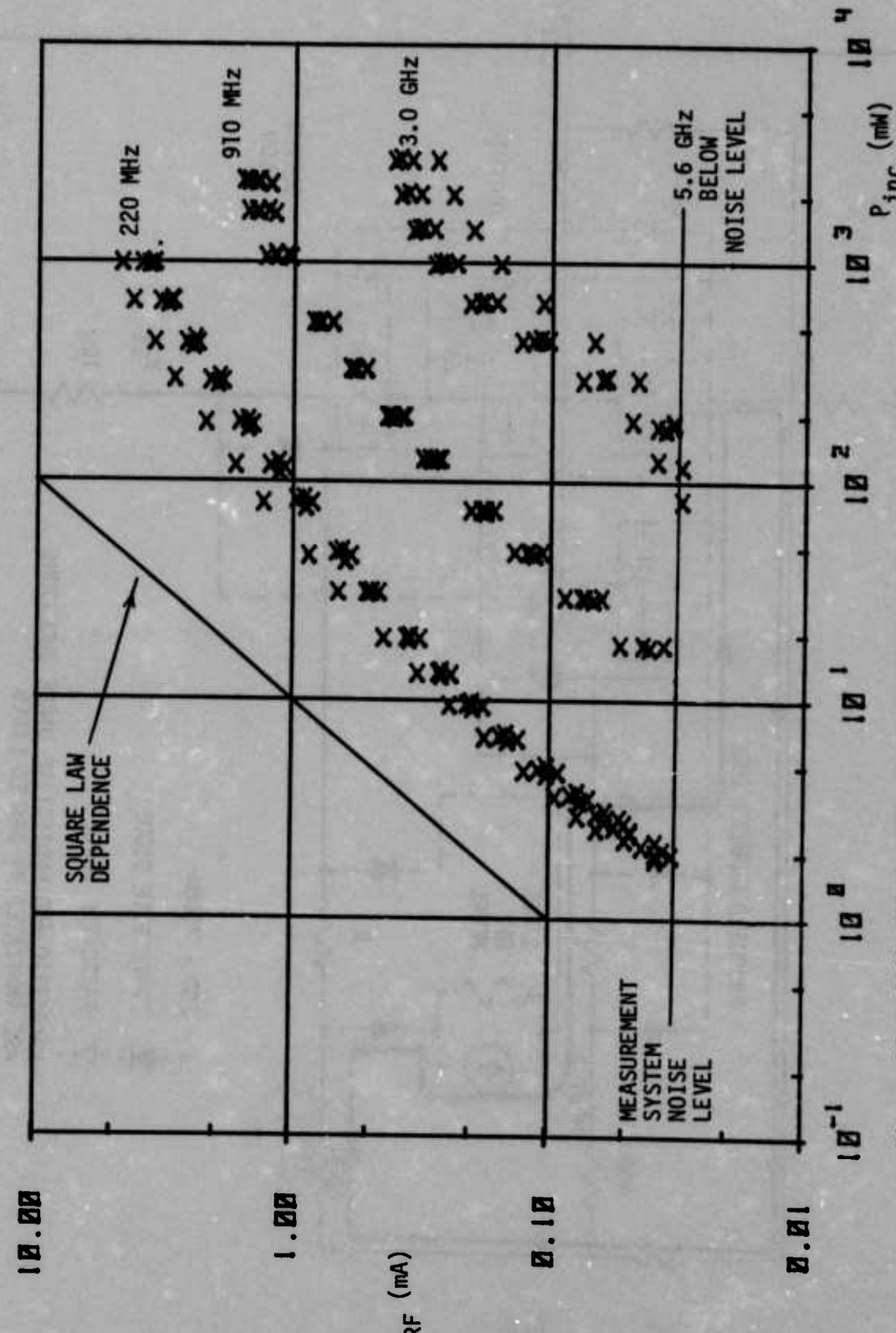

Figure 15 4011 INPUT CIRCUIT RF GENERATED CURRENT CHARACTERISTICS

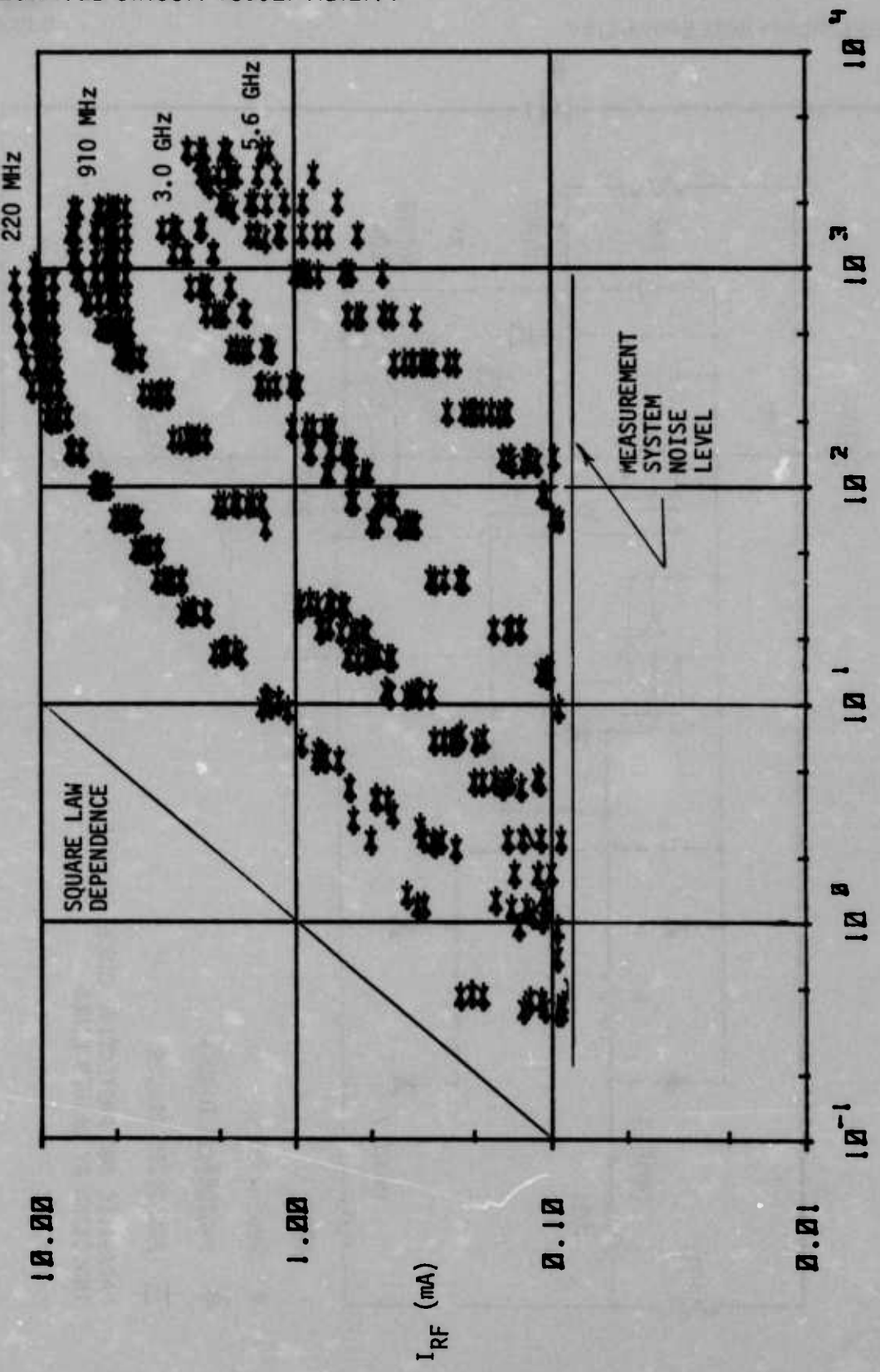

Figure 16 7460 INPUT CIRCUIT RF GENERATED CURRENT CHARACTERISTICS

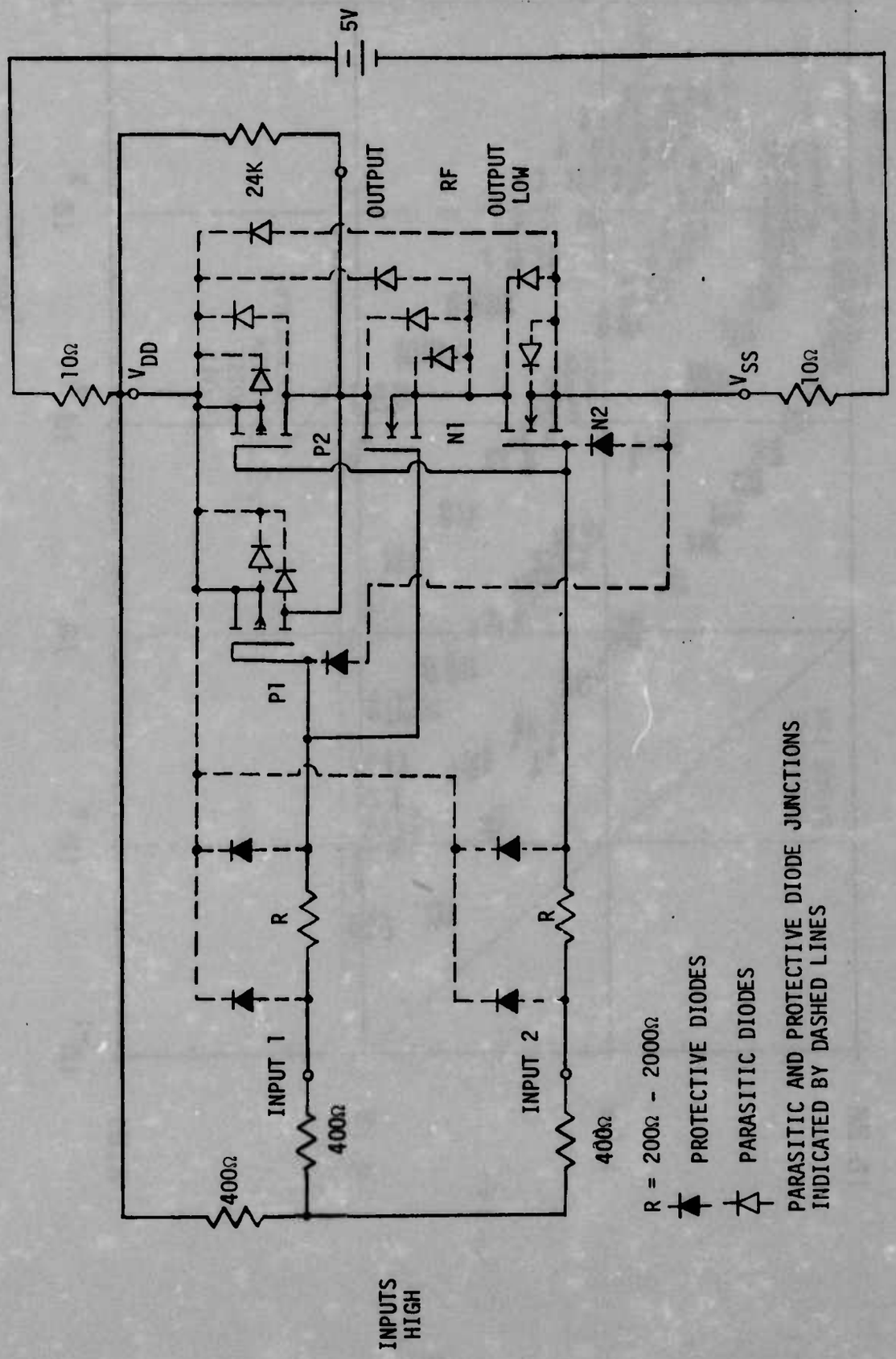

Figure 17 SCHEMATIC DIAGRAM OF 4011 TEST SETUP FOR RF INJECTED INTO THE OUTPUT PORT WITH OUTPUT LOW

identified with their corresponding current loops as shown in figure 18. A MOS device can be thought of as a voltage controlled resistor (the gate voltage controlling the drain-to-source channel resistance). For a given gate voltage, the channel resistance remains constant for low drain-to-source voltages.

Assuming a constant resistance for the two series n channel transistors to V_{SS}, the rectification model predicts that the output voltage can be expressed as a function of the RF power:

$$V_{out} = [I_{Fanout} + I_g(RF)] * [\frac{R_{channel} * R_g(RF)}{R_{channel} + R_g(RF)}]$$

where I_{Fanout} = sink current of the 4011 for the output low configuration.

$I_g(RF)$ = RF generated equivalent Norton current source from the rectification model.

$R_g(RF)$ = equivalent source resistance of the above Norton current source from the rectification model.

$R_{channel}$ = the series resistance of the two series n channel transistors ("on" channel resistance from the output to V_{SS}).

This expression for output voltage contains circuit characteristics (I_{Fanout}), device characteristics ($R_{channel}$), and RF characteristics (I_g (RF), R_G (RF)). Further investigations of these functions will allow a greater understanding of the total circuit RF susceptibility.

The preliminary measurements on the 4011 did not allow time for characterization of $I_g(RF)$ and $R_g(RF)$ for a definitive model. However, assuming a constant resistance for the two series n channels to V_{SS}, an RF generated current can be calculated using the output currents and voltages. The implied current which flows through the two n channels raises the output voltage at 3 GHz to 3 volts. The RF generated currents for the output low, output port injection case in the 4011 and the 7400 are similar. Both the 4011 and the 7400 RF generated currents have an approximate

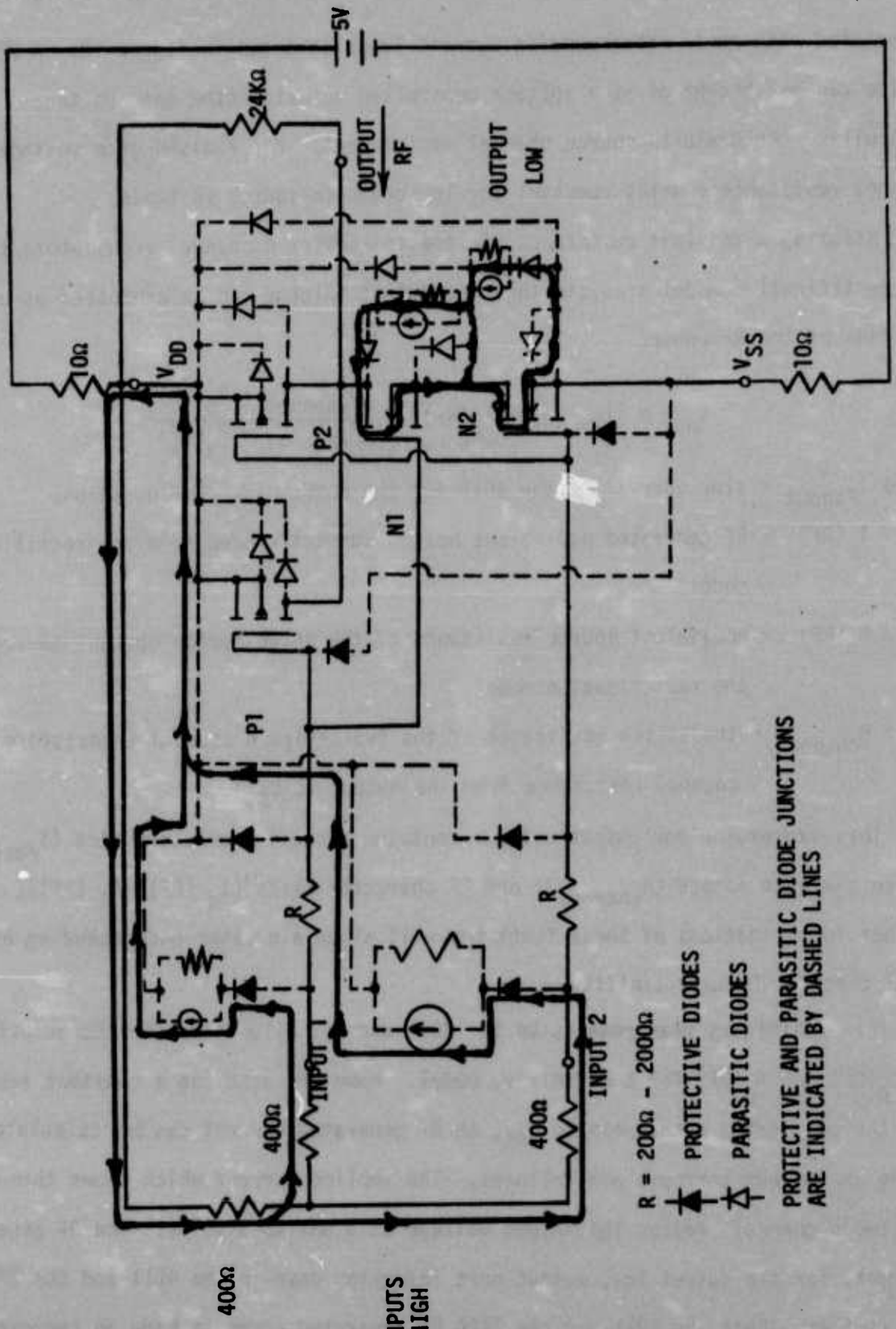

Figure 18 4011 TEST SETUP FOR OUTPUT RF INJECTION SHOWING RF GENERATED CURRENT SOURCES

square law dependence, decrease with increasing frequency, and tend to saturate at high RF levels. These similarities indicate that the bipolar rectification model can reasonably be extended to include MOS devices (due to the presence of parasitic and protective pn junctions).

5. DATA ANALYSIS IMPLICATIONS

The comparison of input voltage, output voltage, and calibration factor for the 4011 and the 7400 is tabulated in Appendix A. These data and the corresponding analyses indicate the susceptibility mechanisms in the 4011 device and possible generalizations to other MOS devices.

5.1 Similarity of 4011 and 7400 RF Effects - The rectification theory used for RF effects in pn junctions in bipolar ICs has been shown to be directly applicable to the parasitic and protective pn junctions in MOS ICs. This bipolar rectification theory has been used to qualitatively explain all significant effects due to injected RF on CMOS 4011 ICs. Additional testing and analyses are required to delineate further this model for the 4011 and other CMOS devices. It now appears that the MOS technology can be treated identically to the bipolar technology in terms of RF susceptibility mechanisms.

5.2 Relative Susceptibility of 4011 and 7400 - The most susceptible configuration for the 4011 is the output low with RF injected into the output port. This configuration is also the most susceptible one for the 7400. A comparison of these configurations, as shown in figure 19, shows that the 7400 is generally more susceptible than the 4011 by a factor of two, although a comparison of individual devices may be quite different. These data are plotted with respect to absorbed RF power in the chip. Calibration factor is essentially the difference in the incident power to the device and the absorbed power in the chip, or the RF rejection properties of the device. The calibration factor for the 7400 is slightly higher than the calibration factor for the 4011 for their most susceptible configurations. This indicates that the total 7400 susceptibility with respect to incident power is slightly greater than the 4011. This is not surprising in light of the proposed

RF INJECTED INTO OUTPUT PORT, OUTPUT LOW

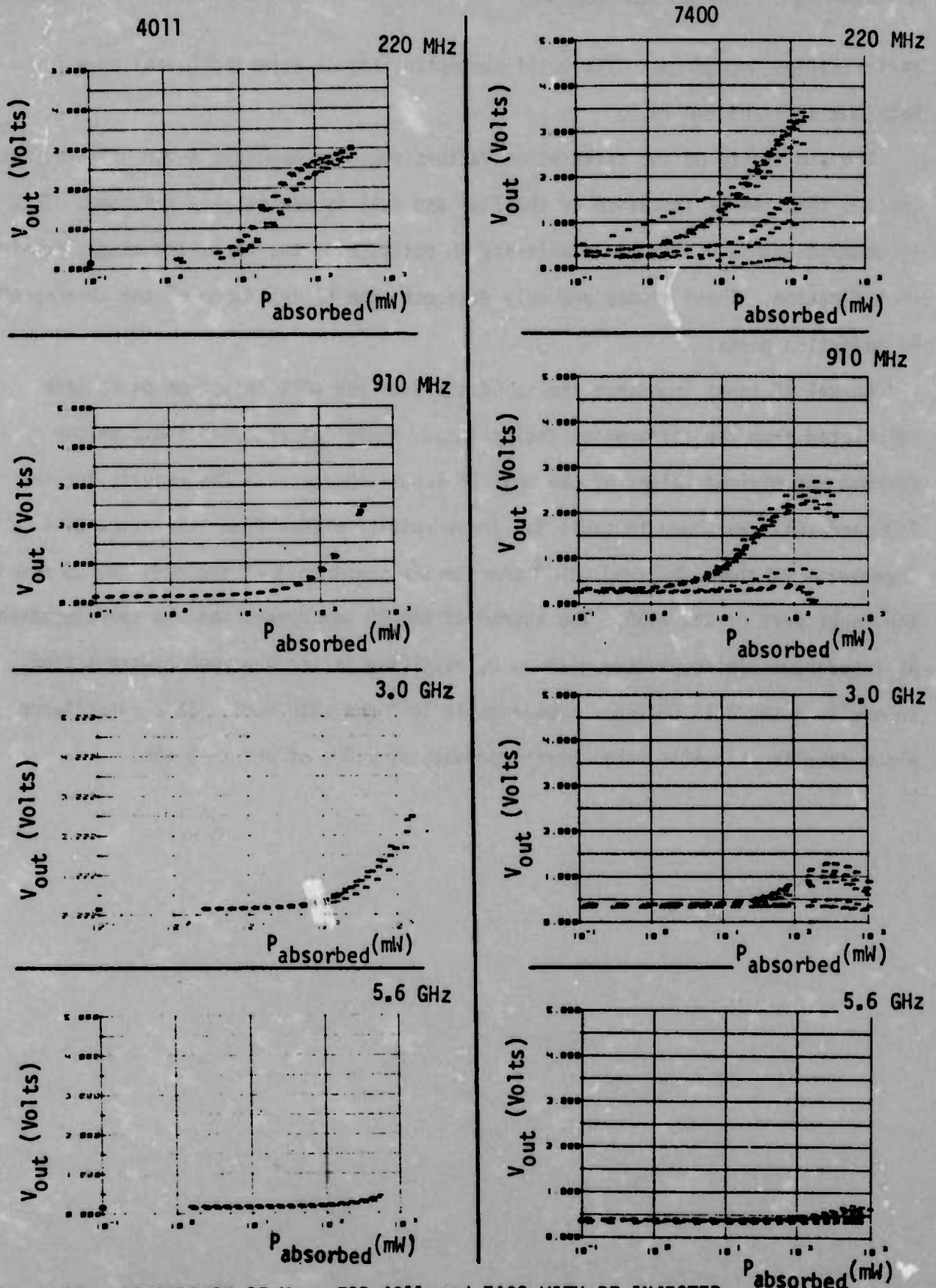

Figure 19 COMPARISON OF V_{out} FOR 4011 and 7400 WITH RF INJECTED INTO OUTPUT PORT, OUTPUT LOW

rectification mechanisms. The total susceptibility is essentially the same for both the 4011 and the 7400.

The similarity of the calibration factors shown in Appendix A for both devices implies that the RF impedance of the 7400 and 4011 is essentially the same. This is understandable due to the similarity in position of the parasitic diodes causing rectification. These diodes probably determine the RF impedance of the corresponding RF injection ports.

Actual RF input impedance limits of the 7400 and 4011 injection ports were calculated from the calibration factor data. These calculations indicate the maximum and minimum values of the real RF input impedances. The results for the 7400 and 4011 are shown in table 3. These results differ from the respective DC impedances of these devices: 10^{12} ohm for the input port of the 4011 and 25 ohm for the input port of the 7400. The source of the DC impedances and the corresponding RF impedances are completely different, resulting in the apparent contradiction. In addition the 4011 DC input impedance is 10^{12} ohm with 5 pf. This capacitance alone results in a 4011 input port impedance at 1 GHz of about 33 ohm.

Table 3 IMPEDANCE RANGES FOR 4011 and 7400

RF INTO GATE INPUT

FREQUENCY (GHz)	4011 IMPEDANCE RANGE (Ω)	7400 IMPEDANCE RANGE (Ω)
0.22	14-182 / 25-102	9-290 / 9-272
0.91	13-190 / 15-155	7-340 / 7-340
3.0	15-171 / 23-110	12-205 / 13-186
5.6	15-166 / 18-135	5-458 / 4-693

KEY

RF INTO GATE OUTPUT

FREQUENCY (GHz)	4011 IMPEDANCE RANGE (Ω)	7400 IMPEDANCE RANGE (Ω)
0.22	20-126 / 16-152	5-458 / 5-458
0.91	13-199 / 9-272	2-1160 / 3-900
3.0	21-120 / 22-113	6-396 / 7-340
5.6	14-172 / 14-176	4-693 / 5-458

6. CONCLUSIONS

The 4011 is slightly less susceptible than the 7400 for their most susceptible configurations (RF injected into the output with the output low). Analysis of RF effects in the 4011 indicate that the RF signal is rectified at the device pn junctions. All significant RF effects can be qualitatively explained using the bipolar rectification theory from the 7400 analyses. All testing indicates that the bipolar rectification theory applies also to MOS devices due to their parasitic and protective pn junctions.

A complete characterization of the significant 4011 pn junctions is required to substantiate all circuit reactions to RF interference. The characterization of these junctions will lead to a model which can probably be extended to other CMOS devices due to similarities in parasitic and protective diode junctions. These similarities may allow a general RF effects model for all CMOS devices made by a given manufacturer.

Further work is also required to examine the relative susceptibility of various CMOS system interfaces. A CMOS-CMOS interface was simulated in the present RF interference testing. Various other CMOS interfaces (CMOS-TTL, TTL-CMOS, HTL-CMOS, etc.) should be studied on a system scale to determine an optimal logic system with respect to RF susceptibility. Linear CMOS devices should also be studied to determine if their RF effects are similar to digital CMOS devices.

All conclusions are constrained to the device, circuit, and assumptions contained in this report. Additional testing and analyses are required to expand and refine these results.

REFERENCES

1. "Integrated Circuit Electromagnetic Susceptibility Investigation - Bipolar NAND Gate Study" MDC Report E 1123 dated 26 July 1974. Prepared under contract No. N00178-73-C-0362 for the U. S. Naval Weapons Laboratory by McDonnell Douglas Astronautics Company - East, St. Louis, Missouri 63166.

2. "Integrated Circuit Electromagnetic Susceptibility Investigation - Development Phase Report" MDC E0690 dated 19 October 1972. Prepared under contract number N00178-72-C-0213 for the U. S. Naval Weapons Laboratory by McDonnell Douglas Astronautics Company - East, St. Louis, Missouri 63166

3. "Integrated Circuit Electromagnetic Susceptibility Investigation - Interim Report No. 1" MDC Report E0883 dated 24 August 1973. Prepared under contract number N00178-73-C-0362 for the U. S. Naval Weapons Laboratory by McDonnell Douglas Astronautics Company - East, St. Louis, Missouri 63166

4. "Integrated Circuit Electromagnetic Susceptibility Investigation - Interim Report No. 2" MDC Report E0981 dated 28 December 1973. Prepared under contract number N00178-73-C-0362 for the U. S. Naval Weapons Laboratory by McDonnell Douglas Astronautics Company - East, St. Louis, Missouri 63166

5. "Integrated Circuit Electromagnetic Susceptibility Investigation - Test and Measurement Systems" MDC Report E1099 dated 12 July 1974. Prepared under contract number N00178-73-C-0362 for the U. S. Naval Weapons Laboratory by McDonnell Douglas Astronautics Company - East, St. Louis, Missouri 63166

APPENDIX A

4011/7400 INTERFERENCE DATA COMPARISON

4011/7400 INTERFERENCE DATA COMPARISON
RF INJECTED INTO INPUT, OUTPUT LOW

4011 220 MHz

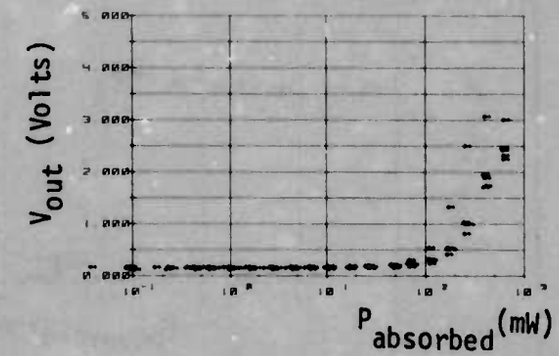

7400 220 MHz

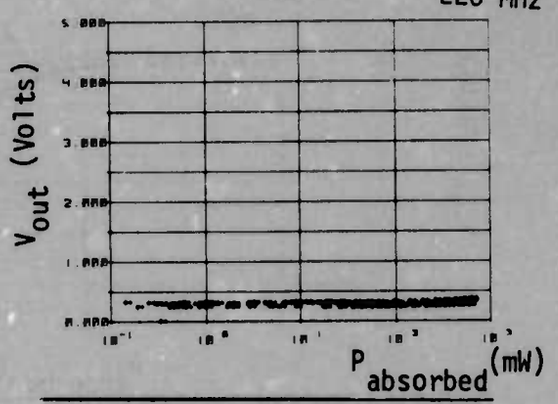

910 MHz

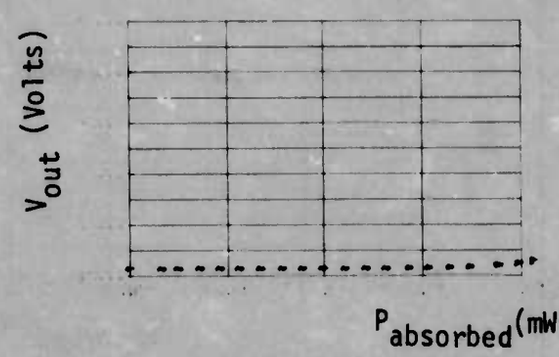

910 MHz

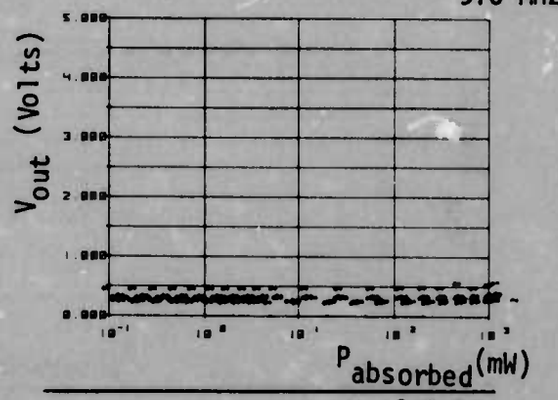

3.0 GHz

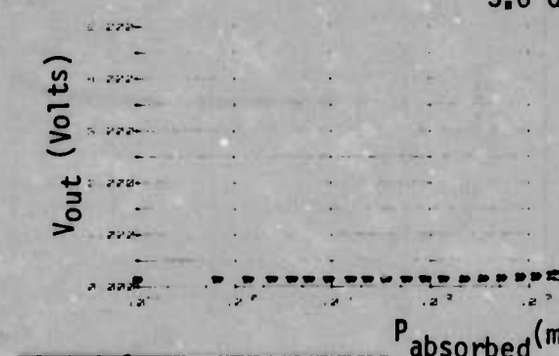

3.0 GHz

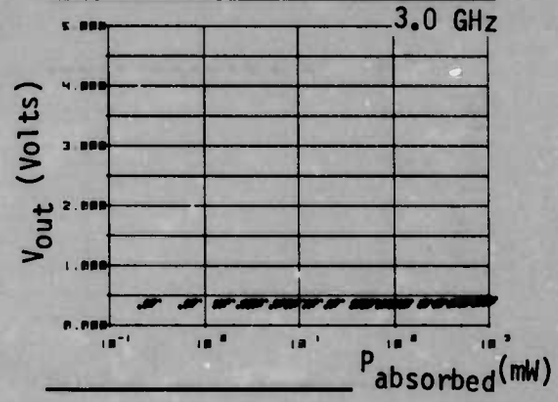

5.6 GHz

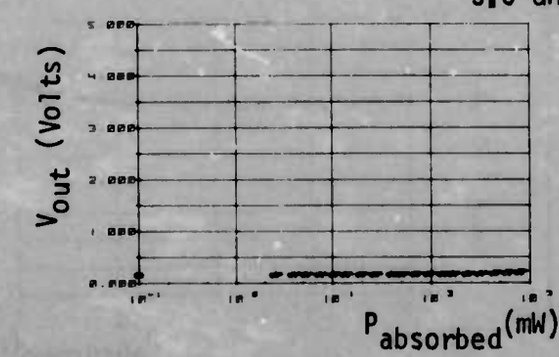

5.6 GHz

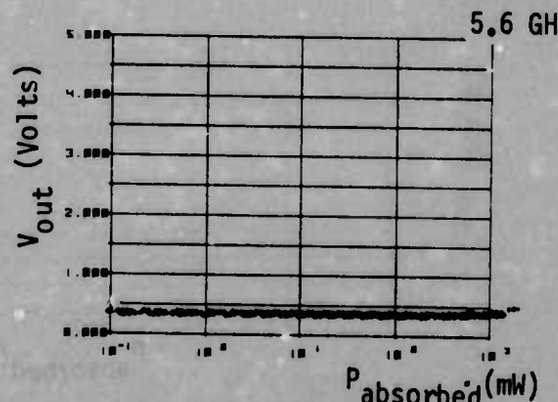

4011/7400 INTERFERENCE DATA COMPARISON
RF INJECTED INTO INPUT, OUTPUT HIGH

4011 — 220 MHz

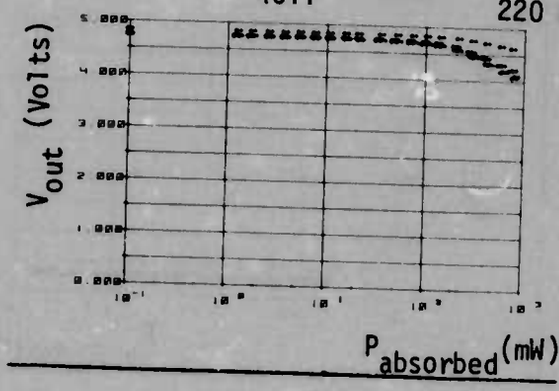

7400 — 220 MHz

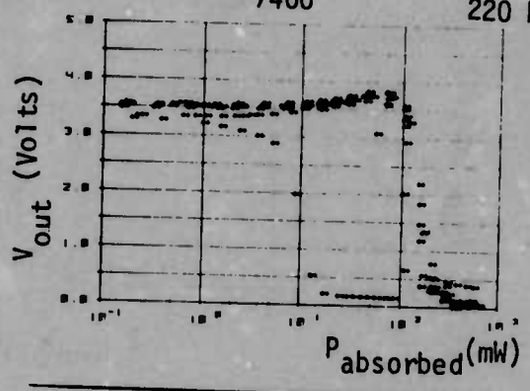

910 MHz

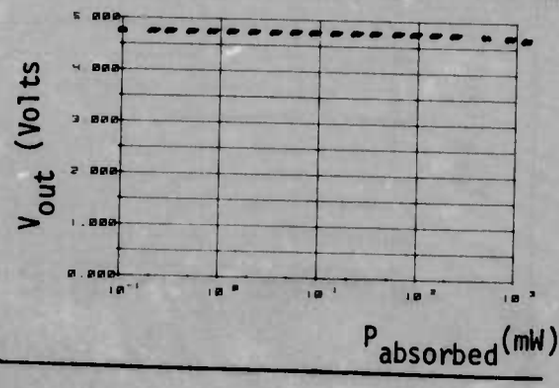

910 MHz

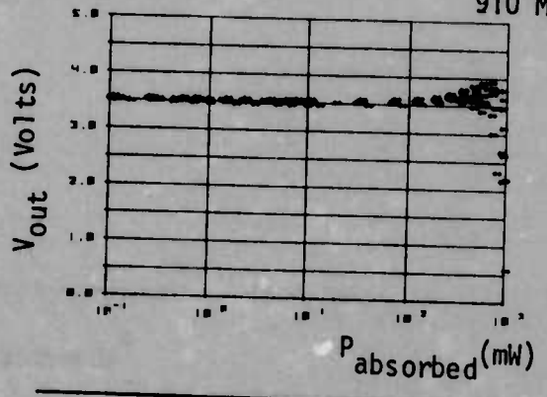

3.0 GHz

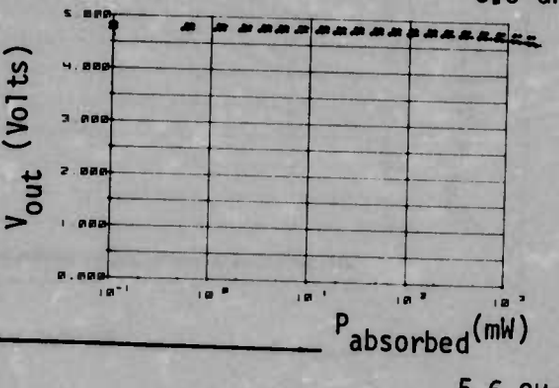

3.0 GHz

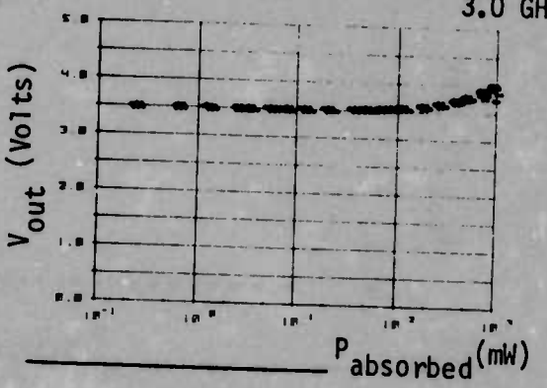

5.6 GHz

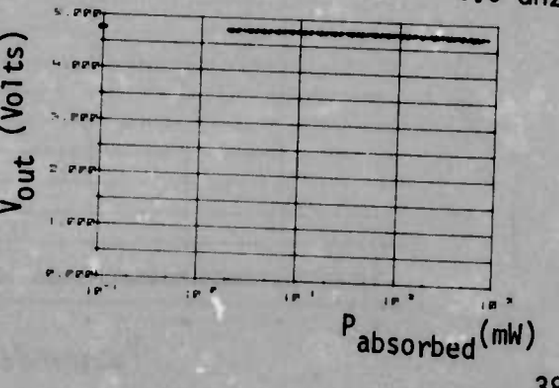

5.6 GHz

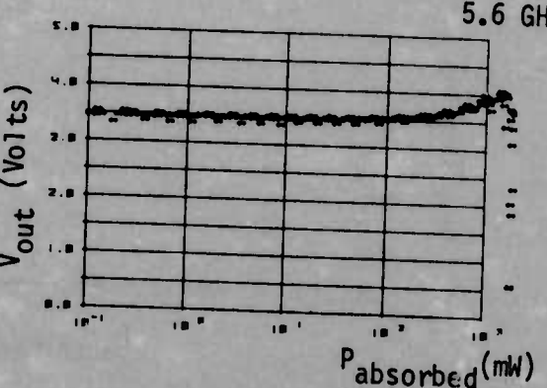

INTEGRATED CIRCUIT SUSCEPTIBILITY

4011/7400 INTERFERENCE DATA COMPARISON
RF INJECTED INTO OUTPUT, OUTPUT LOW

4011

220 MHz

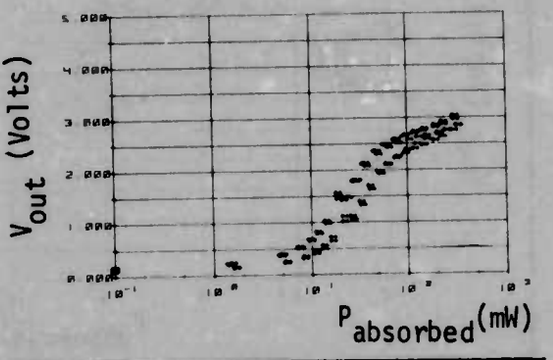

910 MHz

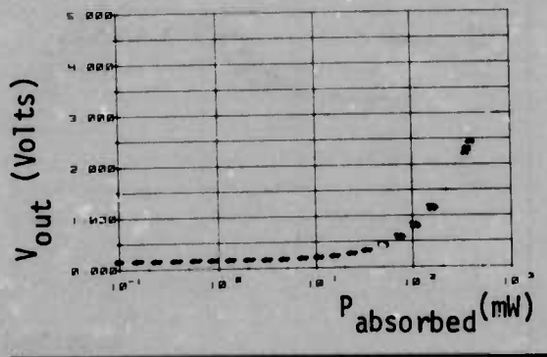

3.0 GHz

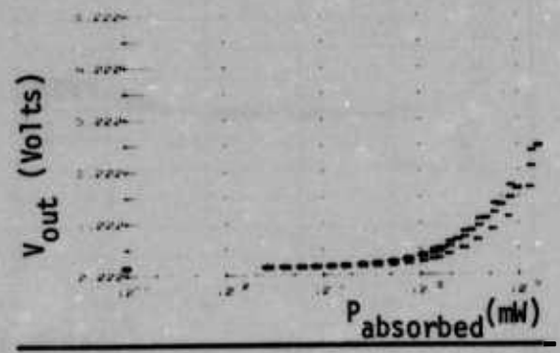

5.6 GHz

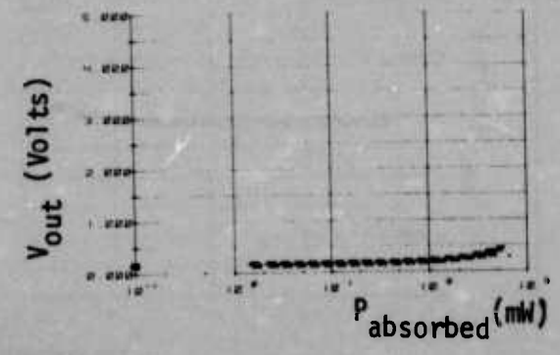

7400

220 MHz

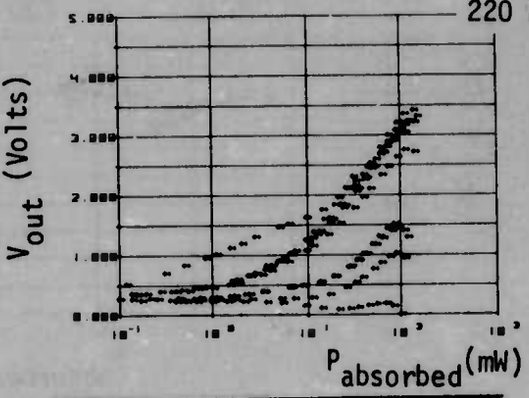

910 MHz

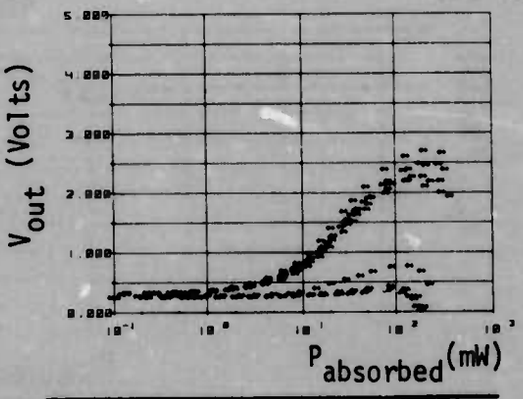

3.0 GHz

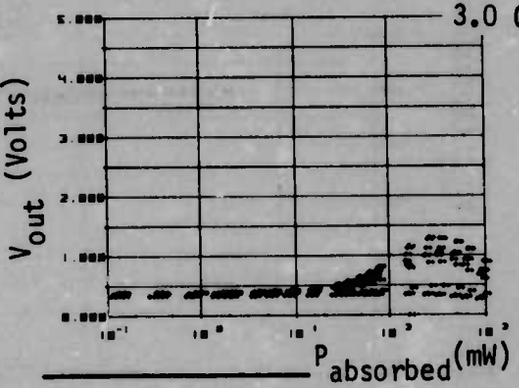

5.6 GHz

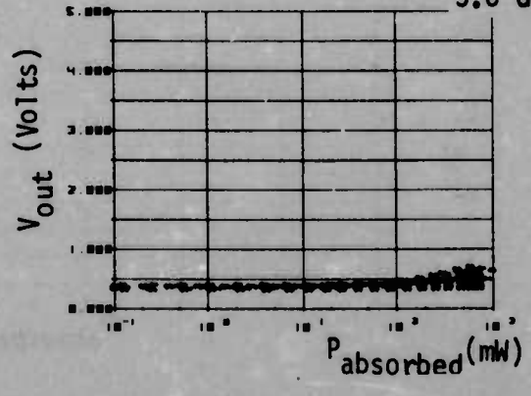

4011/7400 INTERFERENCE DATA COMPARISON
RF INJECTED INTO OUTPUT, OUTPUT HIGH

4011 220 MHz

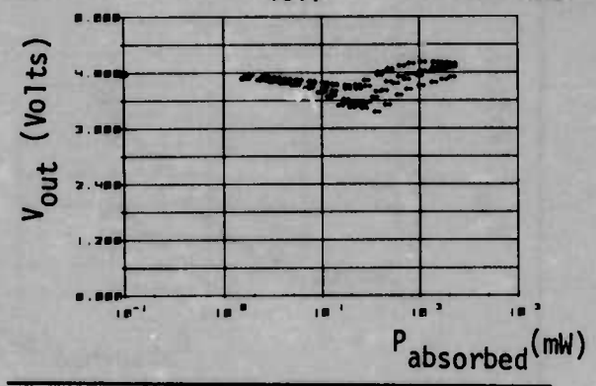

7400 220 MHz

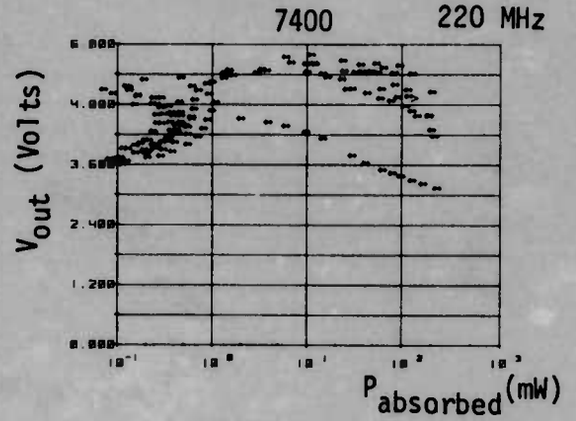

910 MHz

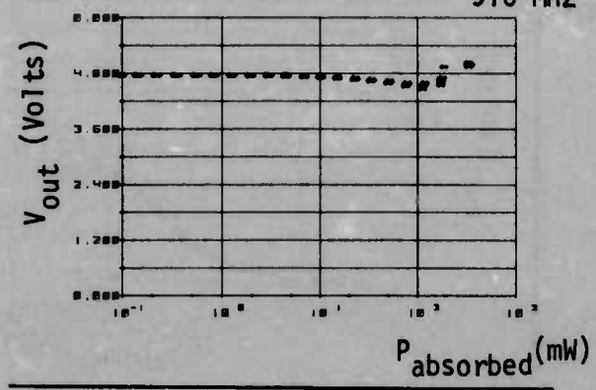

910 MHz

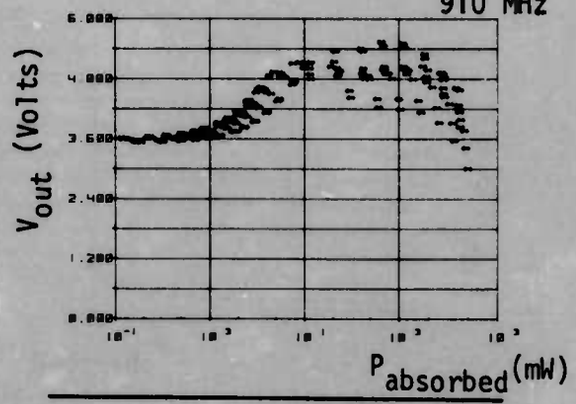

3.0 GHz

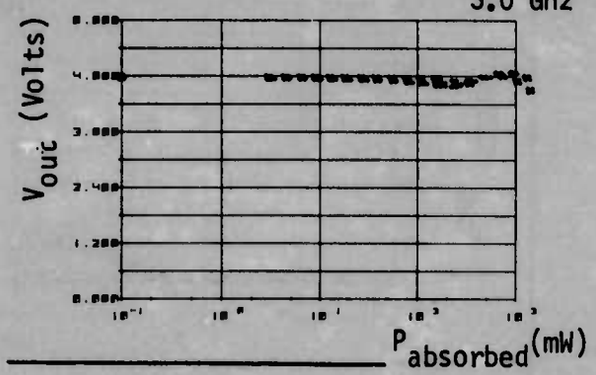

3.0 GHz

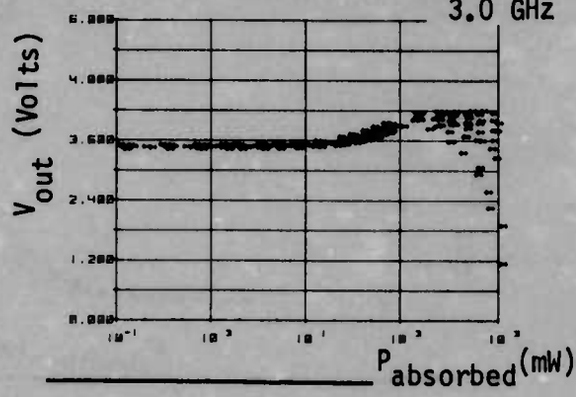

5.6 GHz

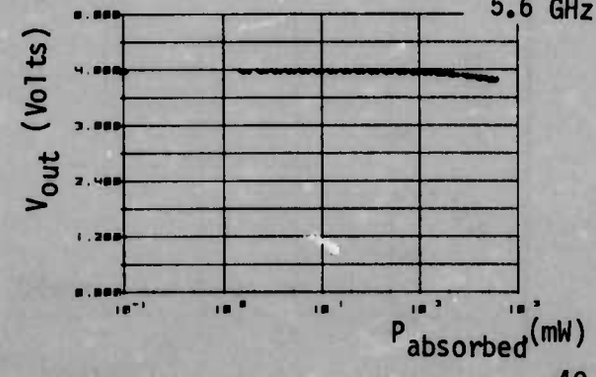

5.6 GHz

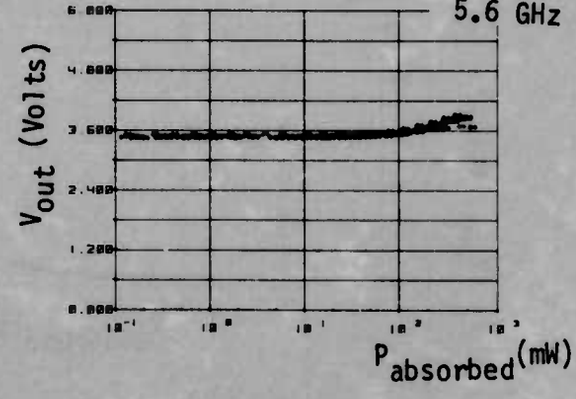

INTEGRATED CIRCUIT SUSCEPTIBILITY

4011/7400 INTERFERENCE DATA COMPARISON

RF INJECTED INTO INPUT. OUTPUT LOW

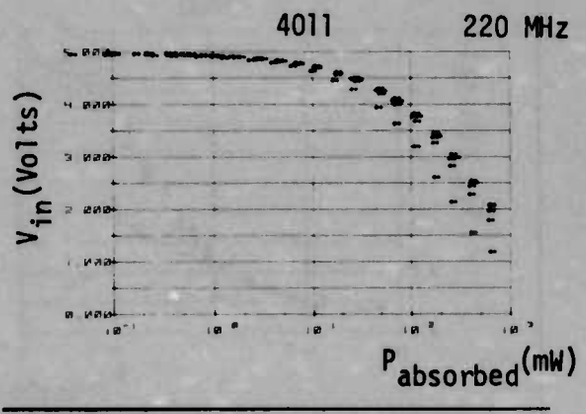

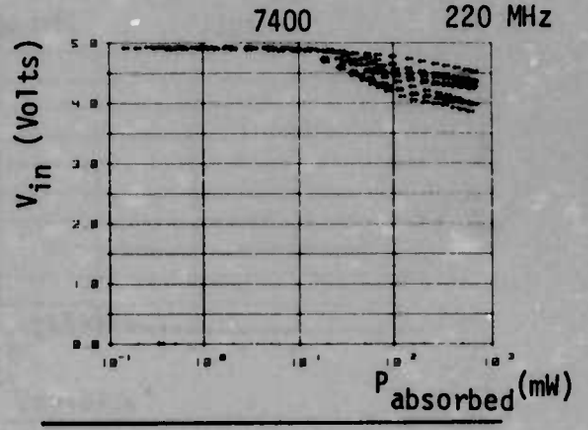

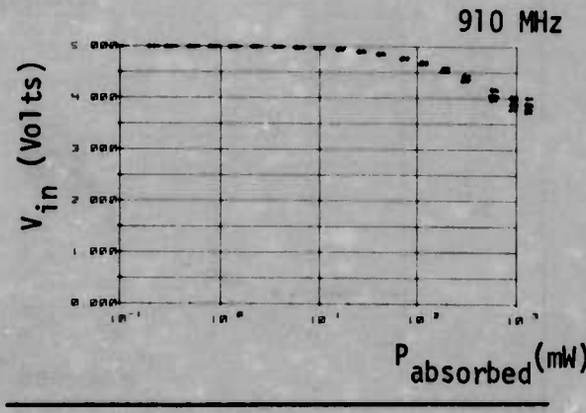

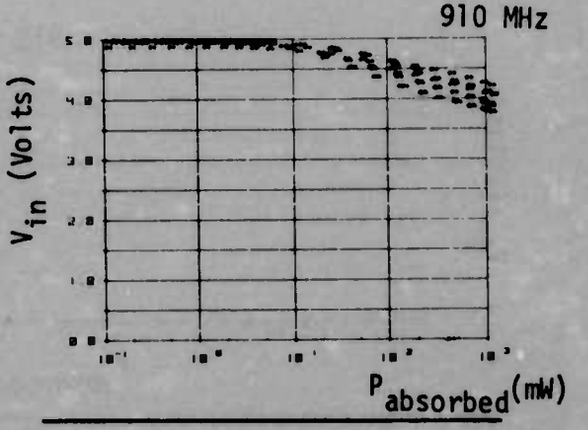

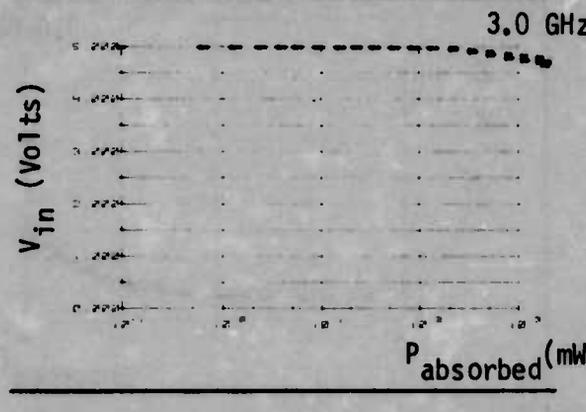

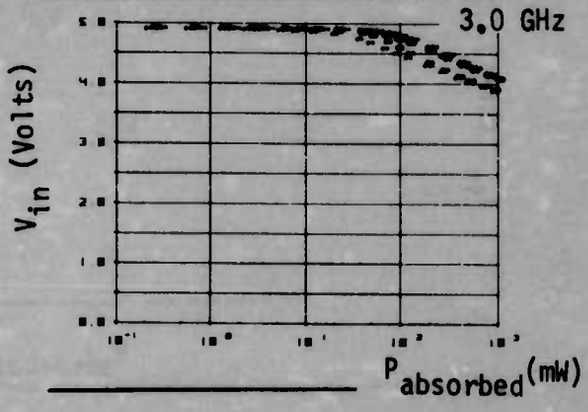

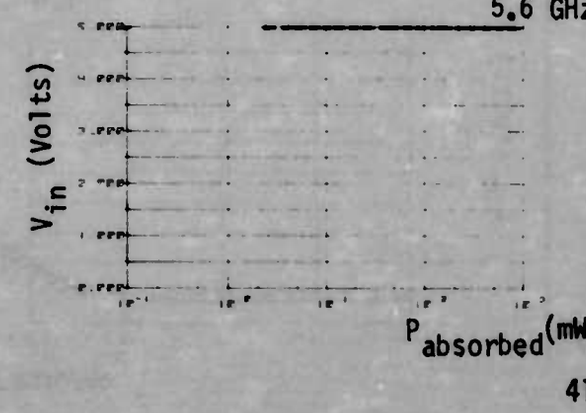

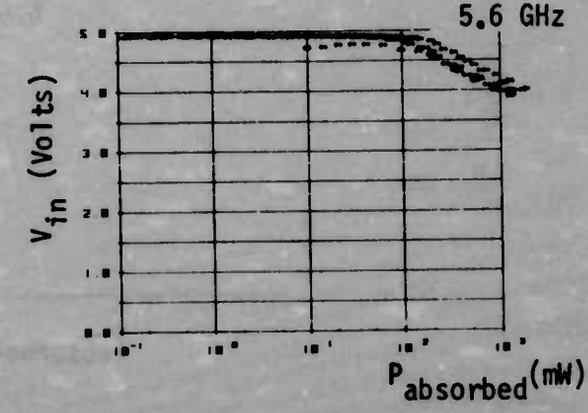

INTEGRATED CIRCUIT SUSCEPTIBILITY

4011/7400 INTERFERENCE DATA COMPARISON
RF INJECTED INTO INPUT, OUTPUT HIGH

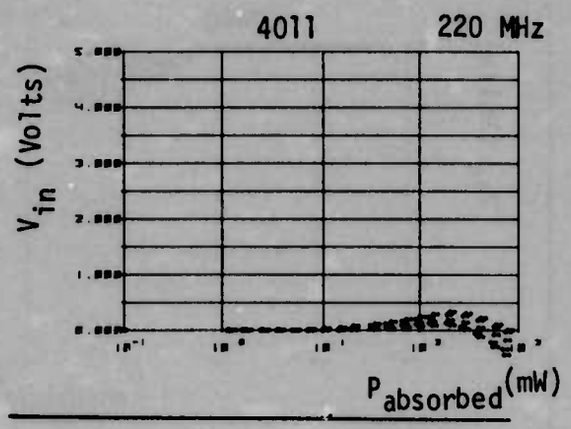

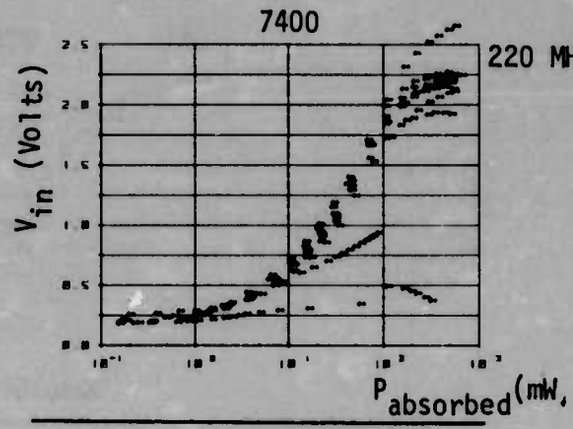

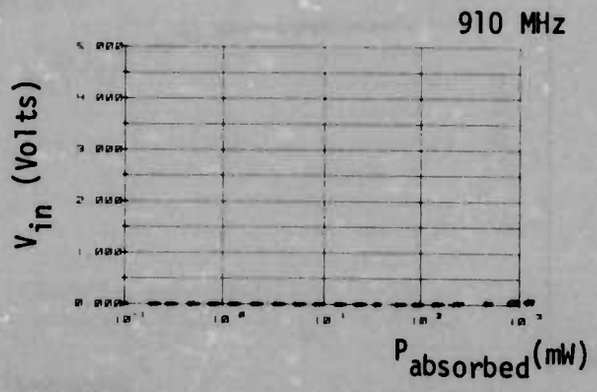

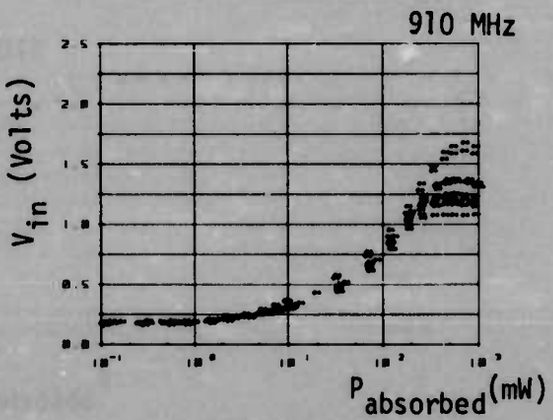

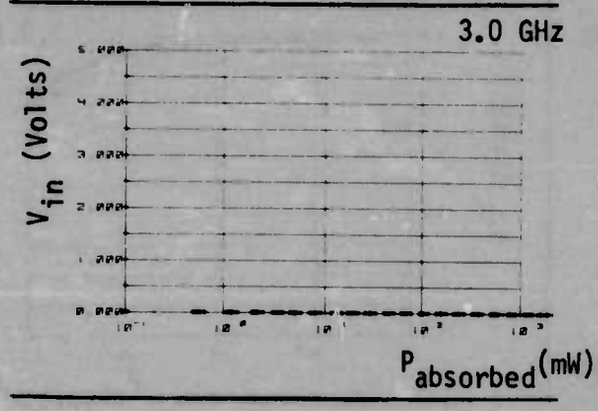

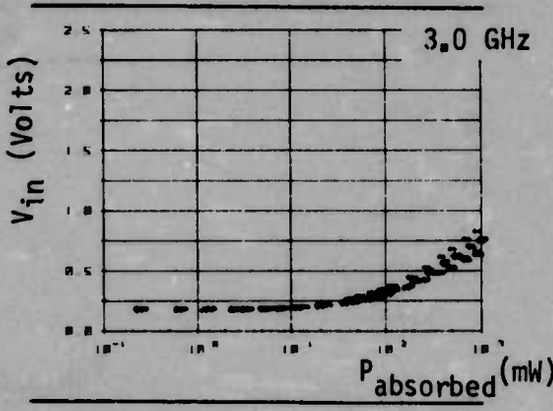

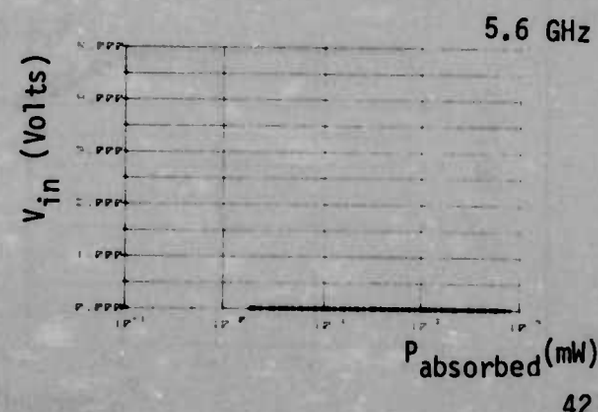

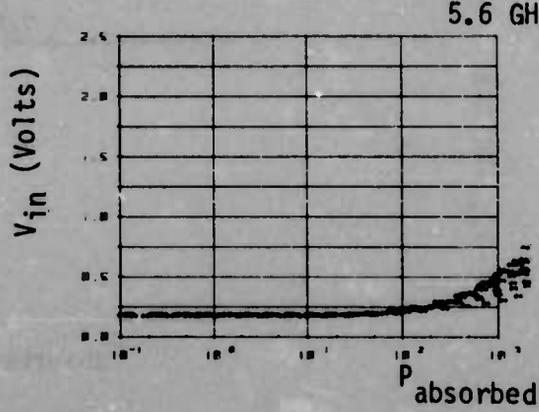

INTEGRATED CIRCUIT SUSCEPTIBILITY

4011/7400 INTERFERENCE DATA COMPARISON
RF INJECTED INTO OUTPUT. OUTPUT LOW

4011 220 MHz

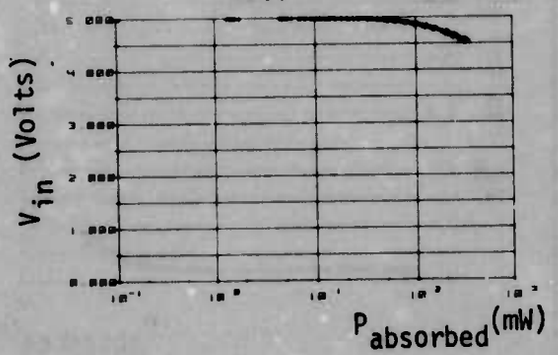

910 MHz

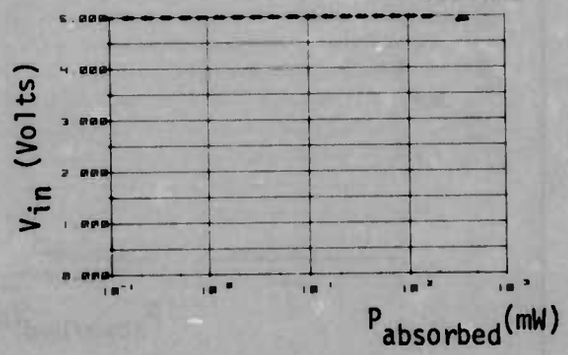

3.0 GHz

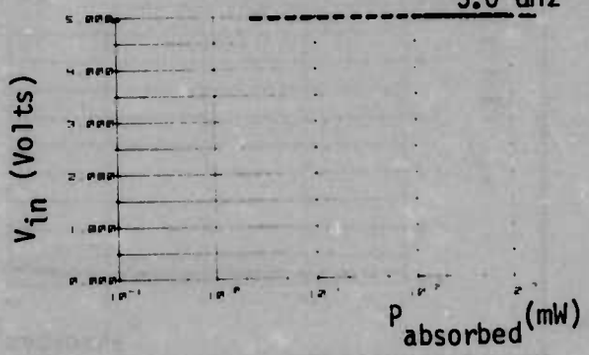

5.6 GHz

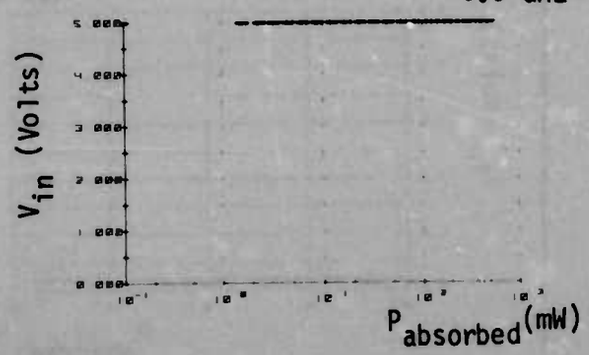

7400 220 MHz

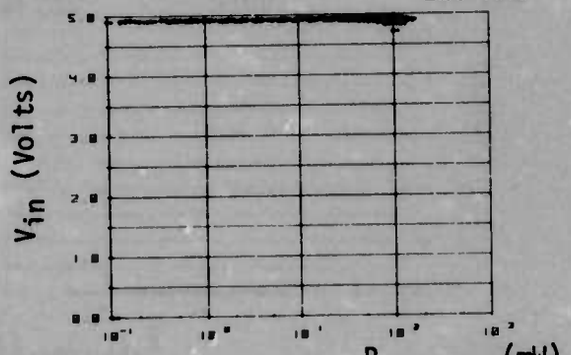

910 MHz

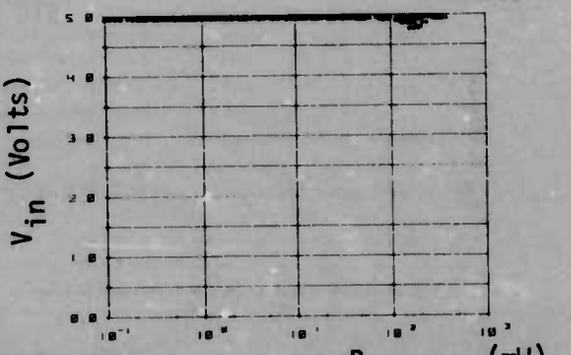

3.0 GHz

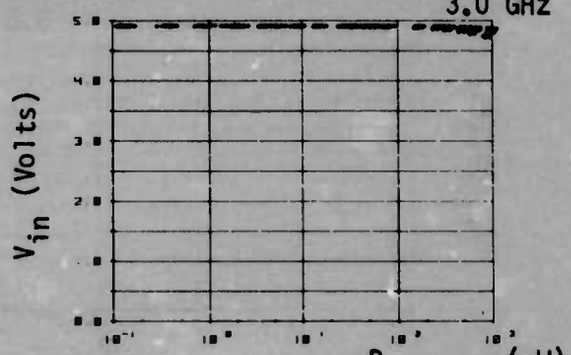

5.6 GHz

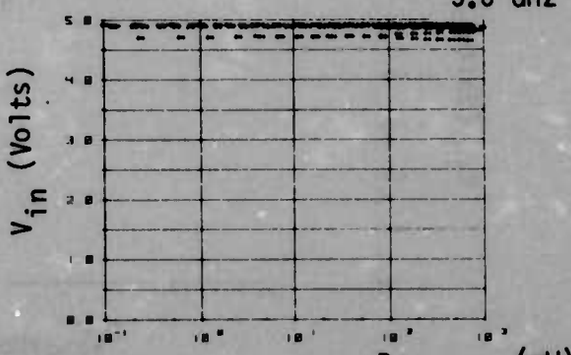

INTEGRATED CIRCUIT SUSCEPTIBILITY

4011/7400 INTERFERENCE DATA COMPARISON
RF INJECTED INTO OUTPUT, OUTPUT HIGH

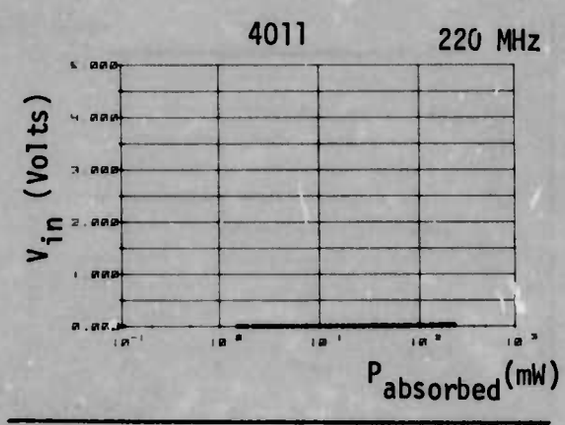

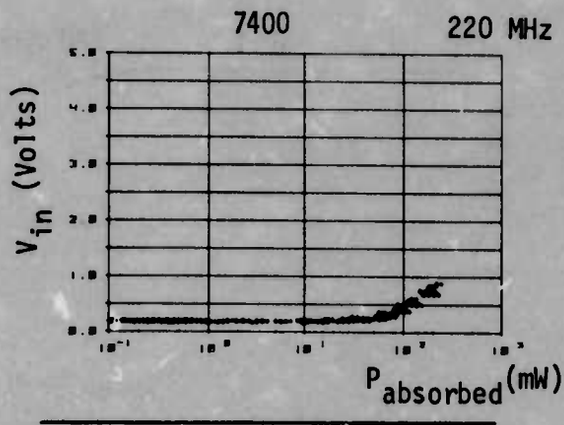

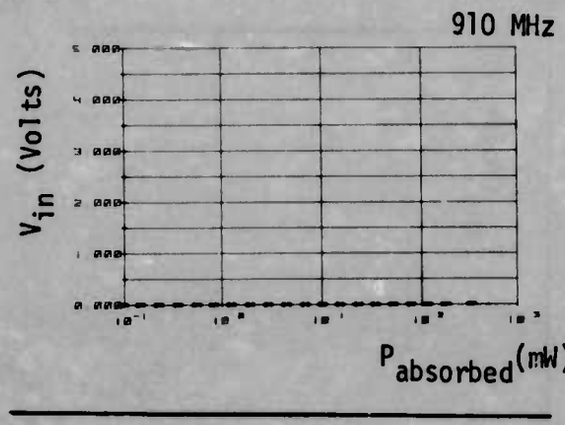

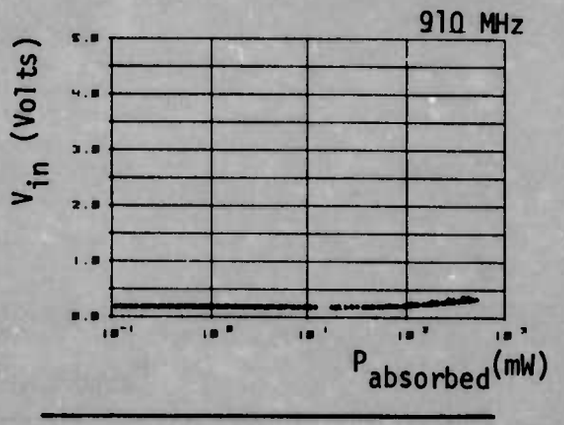

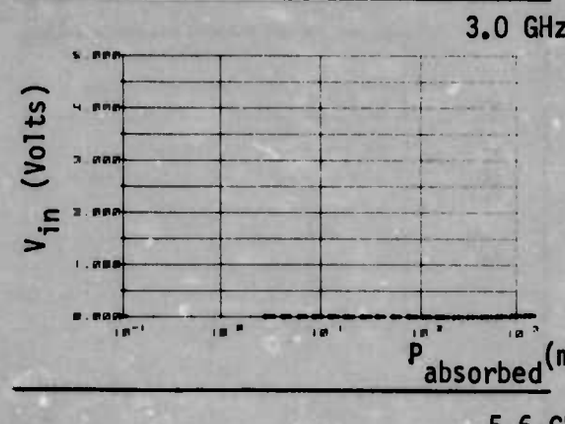

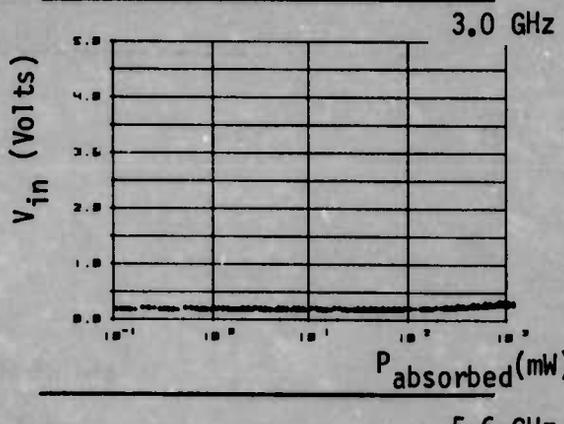

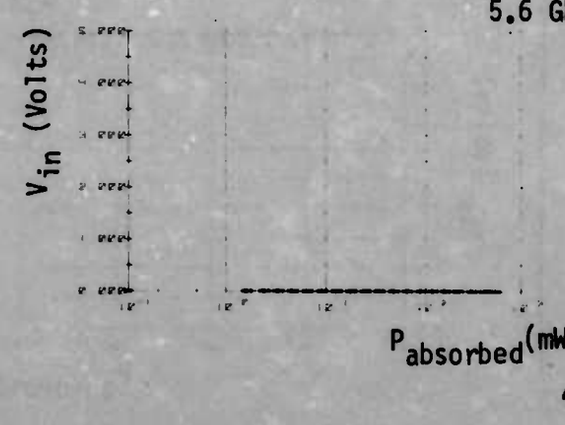

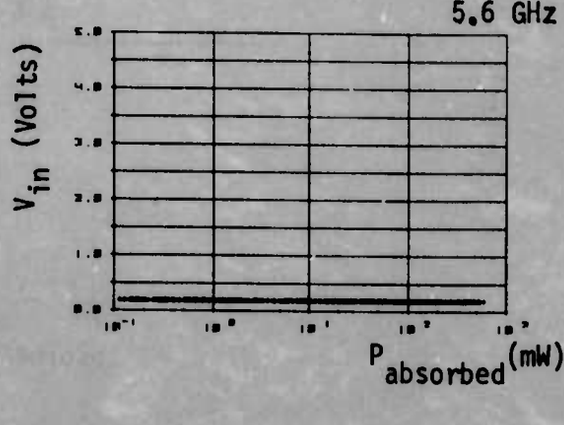

INTEGRATED CIRCUIT SUSCEPTIBILITY

4011/7400 INTERFERENCE DATA COMPARISON

RF INJECTED INTO INPUT, OUTPUT LOW

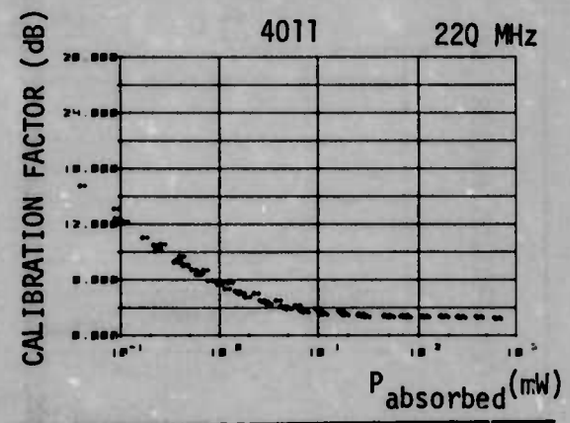

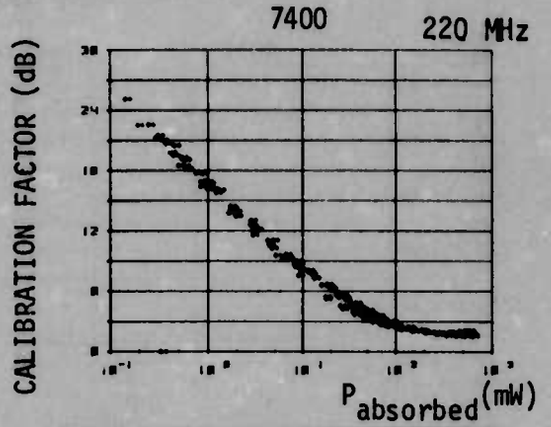

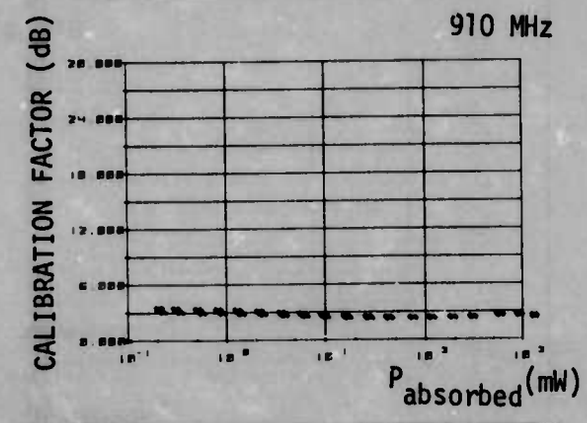

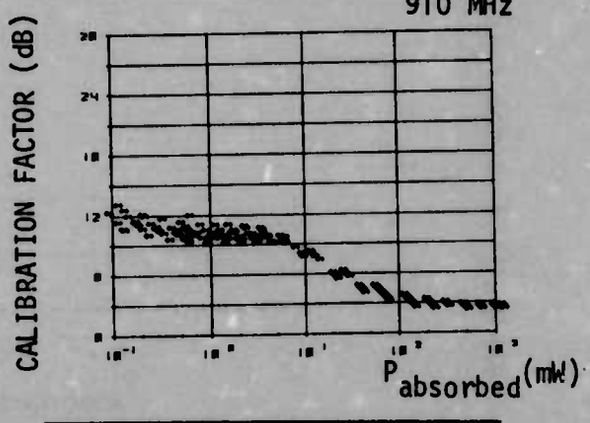

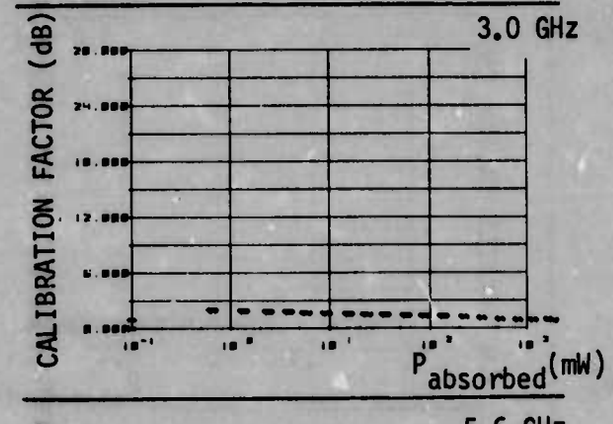

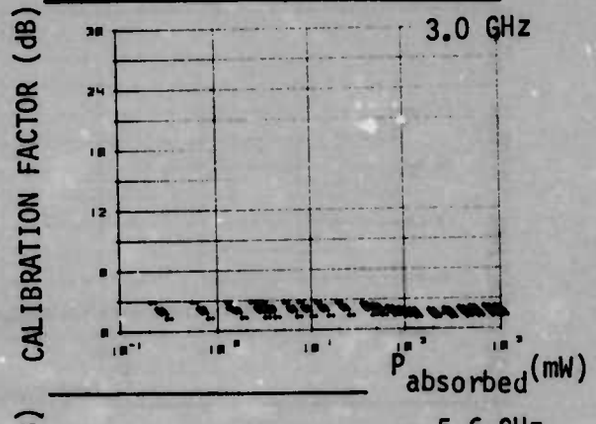

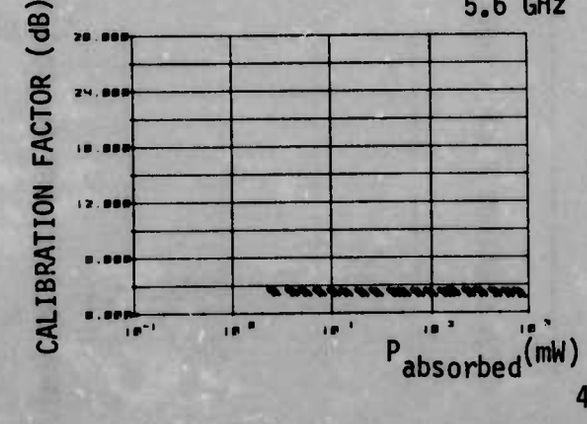

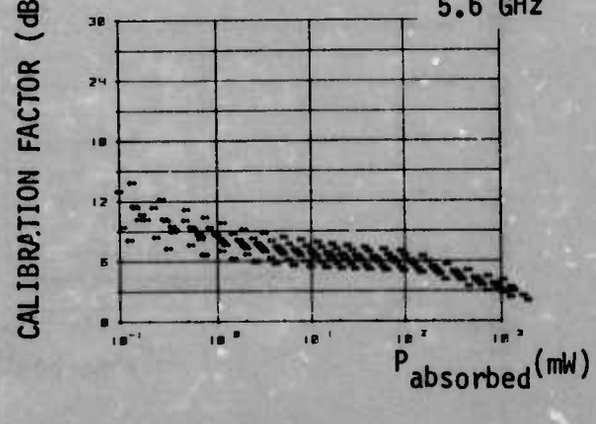

INTEGRATED CIRCUIT SUSCEPTIBILITY

4011/7400 INTERFERENCE DATA COMPARISON
RF INJECTED INTO INPUT, OUTPUT HIGH

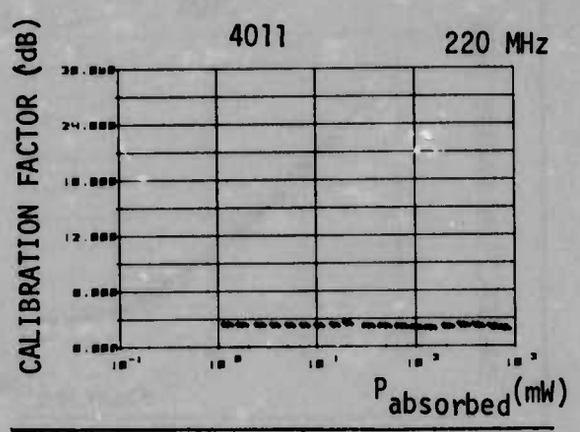

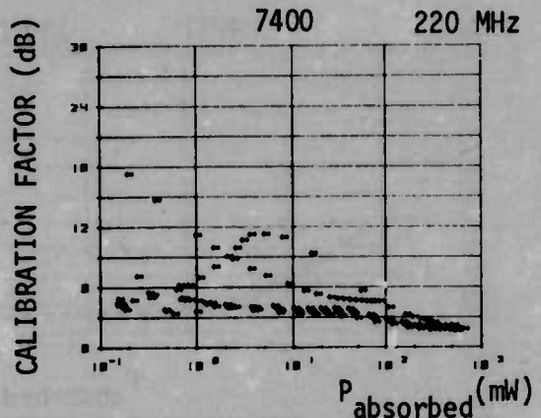

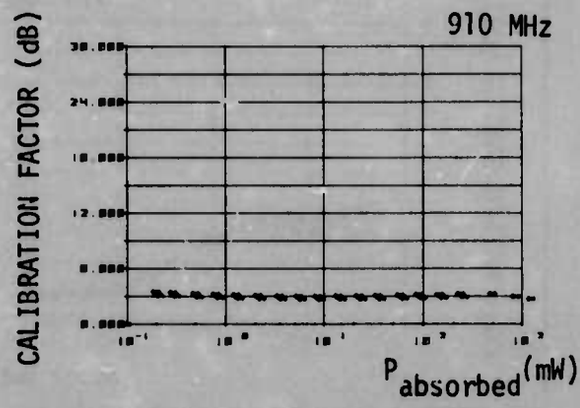

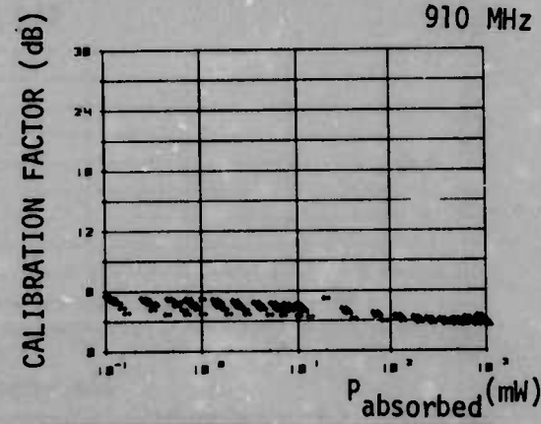

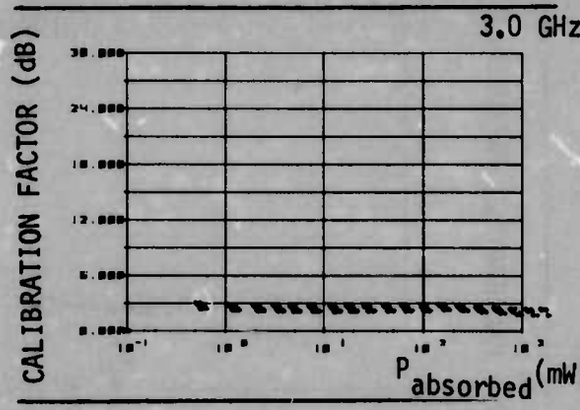

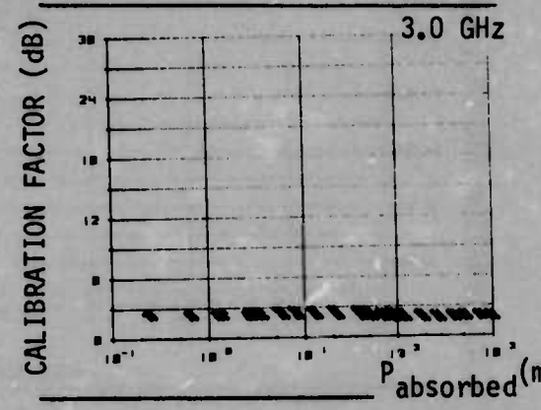

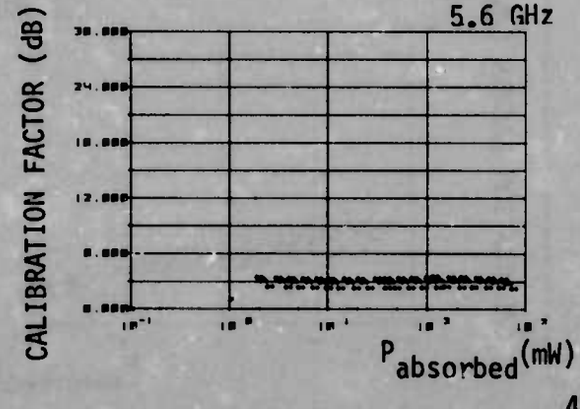

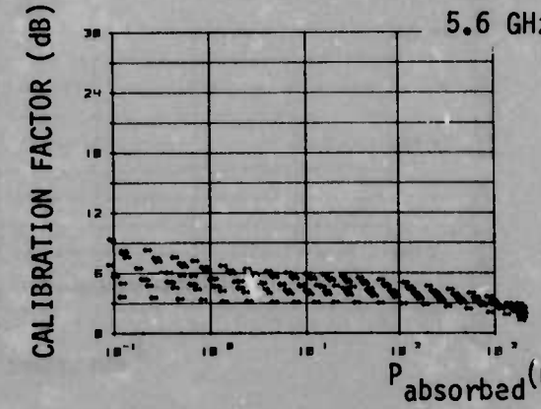

4011/7400 INTERFERENCE DATA COMPARISON
RF INJECTED INTO OUTPUT, OUTPUT LOW

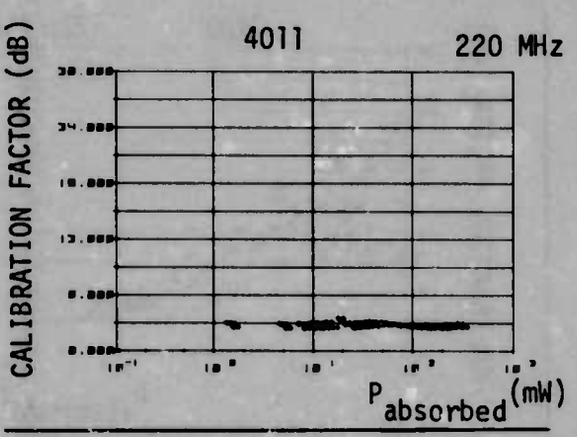

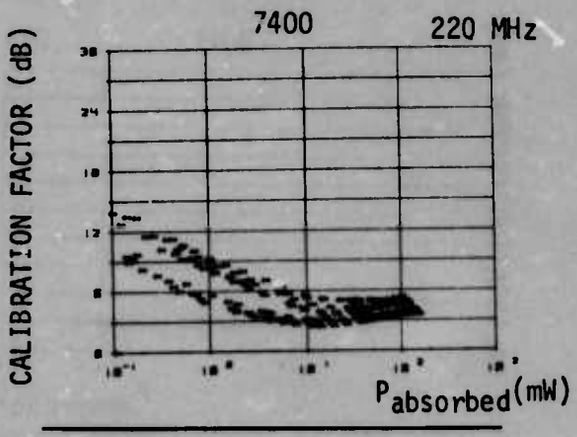

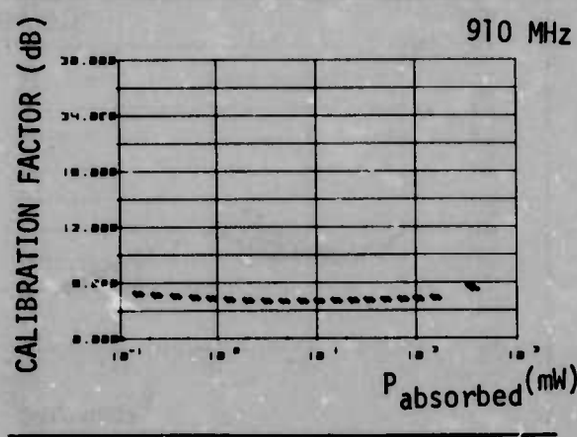

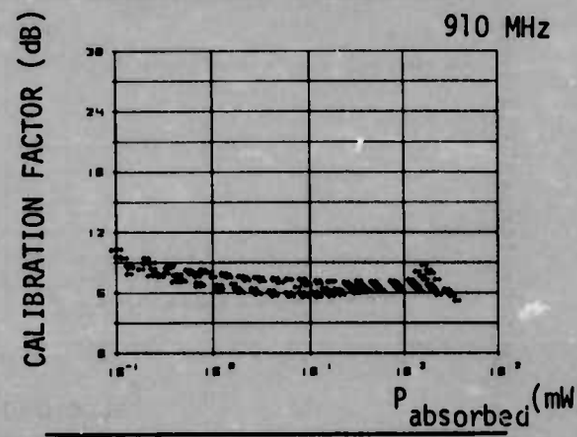

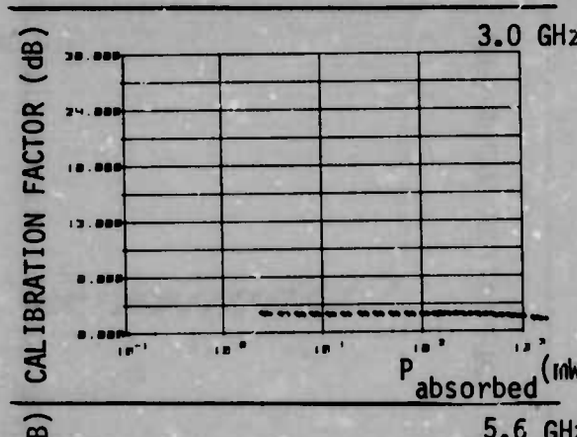

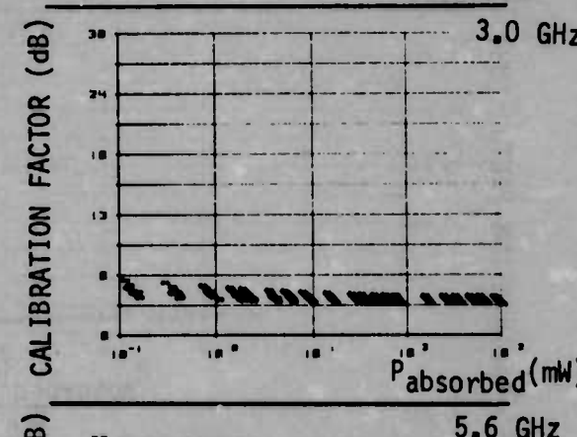

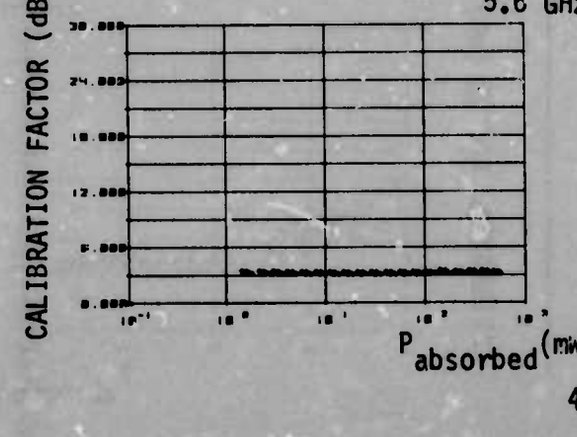

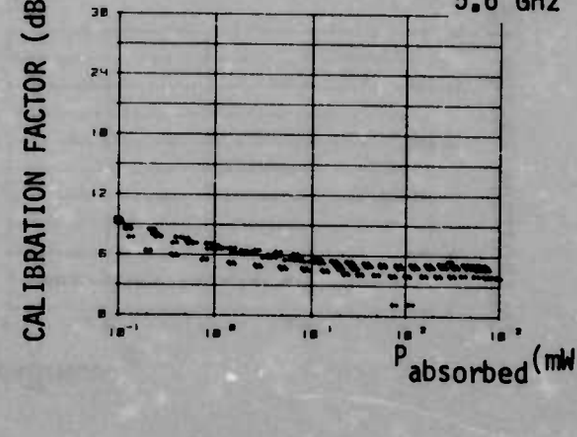

4011/7400 INTERFERENCE DATA COMPARISON
RF INJECTED INTO OUTPUT, OUTPUT HIGH

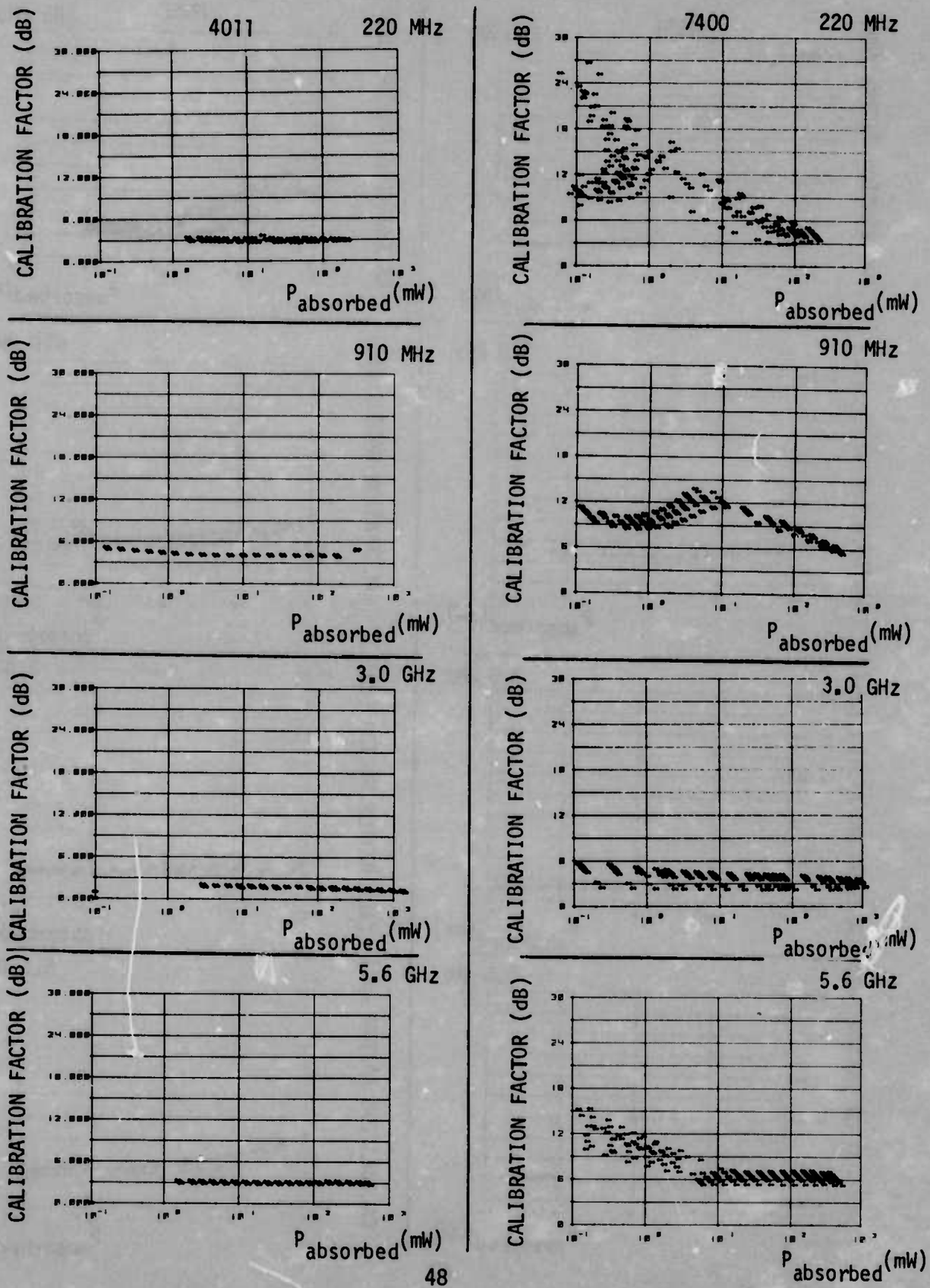

DISTRIBUTION

Executive Office of the President
Office of Telecommunications Policy
Washington, D. C. 20504

ODDR&E
Assistant Director (E&PS)
Attn: Dr. George H. Heilmeier
Pentagon, Room 3D1079
Washington, D. C. 20301

Director, Defense Nuclear Agency
Attn: RAEV (Maj. W. Adams)
Washington, D. C. 20305

Chief of Naval Operations
Attn: OP-932
OP-932C
Washington, D. C. 20350

Chief of Naval Material
Attn: MAT-03423 (Lt. R. Birchfield)
PM7T
Washington, D. C. 20360

Headquarters, U. S. Air Force (RDPE)
Attn: Lt. Col. A. J. Bills
The Pentagon, Room 4D267
Washington, D. C. 20330

Commanding General, U. S. Army Electronics Command
Attn: AMSEL-TL-I (R. A. Gerhold)
NL-C (J. O'Neil)
Ft. Monmouth, New Jersey 07703

Commander, Naval Air Systems Command
Attn: AIR-360G (A. D. Klein)
Washington, D. C. 20360

Commander, Naval Electronic Systems Command
Attn: NAVELEX-095
NAVELEX-3041 (J. A. Cauffman)
NAVELEX-3044 (Navy Member: Advisory Group on Electron Devices, Working Group on Low Power Devices)
NAVELEX-3108 (D. G. Sweet)
NAVELEX-5032 (C. W. Neill)
Washington, D. C. 20360

Commander, Naval Sea Systems Command
Attn: SEA-034
SEA-0341
SEA-06G
Washington, D. C. 20360

Commander, Rome Air Development Center
Attn: RB (J. Scherer)
RBCl (J. Smith)
RBCT (H. Hewitt)
Griffiss Air Force Base
New York 13440

Commander, Air Force Avionics Laboratory
Attn: AFAL/TEA (H. H. Steenbergen)
Wright-Patterson A.F.B., Ohio 45433

Director, Avionics Engineering
Attn: EA (C. Seth)
Wright-Patterson A.F.B.
Dayton, Ohio 45433

Commander, Kirtland Air Force Base
Attn: AFWL/DYX (Dr. D. C. Wunsch)
New Mexico 87117

Commanding Officer, Harry Diamond Laboratory
Attn: J. Sweton
W. L. Vault
H. Dropkin
Washington, D. C. 20438

Commander, Naval Electronics Laboratory Center
Attn: Code 4800 (Dr. D. W. McQuitty)
(A. R. Hart)
San Diego, California 92152

Commander, Naval Ordnance Laboratory
Attn: Code 431 (Dr. M. Petree)
(Dr. J. Malloy)
(R. Haislmaier)
White Oak
Silver Springs, Maryland 20910

Commander, Naval Weapons Center
Attn: Code 5531 (D. Cobb)
Code 5535 (H. R. Blecha)
China Lake, California 93555

Reliability Analysis Center
Rome Air Development Center
Attn: RBRAC (I. Krulac)
Griffiss Air Force Base, New York 13441

Commanding Officer, Electromagnetic Compatibility
Analysis Center (ECAC)
Attn: CDR Case
J. Atkinson
North Severn
Annapolis, Maryland 21402

Department of the Navy
Attn: Code 7624 (J. Ramsey)
Naval Ammunition Depot
Crane, Indiana 47522

Commander, Naval Electronics Systems Test and
Evaluation Facility
Attn: M. Gullberg
Webster Field
St. Inigoes, Maryland 20684

Naval Post Graduate School
Attn: Code AB (Dr. R. Adler)
Monterey, California 93940

National Bureau of Standards
Attn: J. French
H. Schafft
Washington, D. C. 20234

Dr. James Whalen, Room 2B
4232 Ridge Lea Road
State University of New York at Buffalo
Amherst, New York 14226

The Rand Corporation
Attn: A. L. Hiebert
1700 Main St.
Santa Monica, California 90406

Fairchild Research and Development
Attn: Dr. J. M. Early
M/S 30-0200
4001 Miranda Ave.
Palo Alto, California 94303

RCA Laboratories
Director, Solid State Technology Center
Attn: Dr. G. B. Herzog
Princeton, New Jersey 08540

Mr. J. S. Kilby
5924 Royal Lane
Suite 150
Dallas, Texas 75230

Dr. Gordon E. Moore, V.P.
Intel Corp.
3065 Bowers Road
Santa Clara, California 95051

Bell Telephone Laboratories
Attn: Dr. G. E. Smith
Unipolar Design Department
600 Mountain Avenue
Murray Hill, New Jersey 07974

Automation Industries
Vitro Laboratories Division
Attn: T. H. Miller
14000 Georgia Ave.
Silver Springs, Maryland 20910

Braddock, Dunn, and McDonald, Inc.
Attn: J. Schwartz
First National Bank-East (17th Floor)
Albuquerque, New Mexico 87108

R&D Associates
Attn: Dr. W. Graham
P. O. Box 3480
Santa Monica, California 90406

Illinois Institute of Technology Research Institute
Attn: Dr. Weber
10 West 35th St.
Chicago, Illinois 60616

Research Triangle Institute
Attn: Dr. M. Simons
Dr. Burger
Research Triangle Park,
North Carolina 27709

Defense Documentation Center
Cameron Station
Alexandria, Virginia 22314

Secretariat, Advisory Group on Electron Devices
Attn: W. Kramer, Working Group B
201 Varick St.
New York, New York 10014

LOCAL DISTRIBUTION

C

D

E

EPA/Hooker

F

FC

FE

FG

FV

FVE

FVN

FVR

G

GB

GBP

GBR

MIL

MIM